MASS TRANSFER WITH CHEMICAL REACTION

MASS TRANSFER WITH CHEMICAL REACTION

By

ANTHONY Y. YAU

A Thesis

Submitted to the Faculty of Graduate Studies

in Partial Fulfilment of the Requirements

for the Degree

Master of Engineering

McMaster University

March, 1966

MASTER OF ENGINEERING (1966) McMASTER UNIVERSITY
(Chemical Engineering) Hamilton, Ontario

TITLE: Mass Transfer With Chemical Reaction

AUTHOR: Anthony Yukseen Yau, B.Sc. (Queen's University)

SUPERVISORS: Dr. A. I. Johnson and Dr. A. E. Hamielec

NUMBER OF PAGES: xi, 98

SCOPE AND CONTENTS:

A continuous bubble reactor was used to study the transfer of oxygen into solutions of acetaldehyde. The reaction was catalysed by cobaltous acetate. The parameters investigated included temperature, catalyst concentration, air flow rate and column height.

A mathematical model based on Houghton's work (36) was used to describe the absorption rate in the bubble column. The equation derived was solved numerically. The Sherwood numbers predicted by the theory were compared with those obtained experimentally.

NOMENCLATURE

a	bubble surface area per unit column height, cm/sec
A	constant
A'	cross-sectional area of imaginary air cylinder in Figure A-1b. cm^2
B	constant
c	solubility of oxygen in ethyl acetate, g.mole/c.c.
C	concentration of solute in bulk of liquid, dimensionless or g.mole/c.c.
C_i	concentration of solute at interface g. mole/c.c.
C_s	saturation concentration of solute in liquid phase, dimensionless or g.mole/c.c.
d	diameter of bubble, cm.
d_o	diameter of nozzle, cm.
D	diffusivity, $cm^2/sec.$
D_e	diameter of a sphere whose volume equals that of bubble, cm.
f	bubble frequency, min^{-1}
g	gravitational acceleration, $cm./sec.^2$
G	air flow rate, c.c./sec.
G_N	nitrogen flow rate, c.c./sec.
h	column height, cm.
H	Henry's law constant
ΔH^v	heat of vaporization, cal./g. mole

k	mass-transfer coefficient
k', k'', k'''	reaction rate constants
k_1	first order reaction rate constant, sec.$^{-1}$
k_G, K_G	gas phase mass-transfer coefficient, mole O_2/cm.^{2} sec.
k_L, K_L	liquid phase mass-transfer coefficient, cm./sec.
M	molecular weight
n	number of bubbles in liquid column
N	rate of mass transfer, g.mole/sec.
p	partial pressure of solute, atm.
p_B	partial pressure of non-diffusing gas B, atm.
p_{BM}	log mean pressure of non-diffusing gas B at phase boundary and p_B in the bulk of liquid, atm.
p_i	partial pressure of solute at interface, atm.
p_e	partial pressure of solute over a solution having the concentration of the main stream composition C., atm.
p^o	vapour pressure of solute, atm.
P	total pressure, atm.
r	distance from centre of bubble, cm.
R	gas constant = 1.98, cal./g. mole°K.
R_b	$D_e/2$, cm.
S	bubble surface area, cm.^{2}
S_e	equivalent bubble surface area, cm.^{2}

t	time, sec.
t_e	time of exposure, sec.
T	absolute temperature, °K.
T_b	normal boiling point, °K.
U	main stream velocity, cm./sec.
v_r	bubble velocity of rise, cm./sec.
V	molal volume of solute at normal boiling point, c.c./g.mole
V_B	volume of a single bubble, $cm.^3$
V_r	radial velocity component, dimensionless or cm./sec.
V_R	volume of liquid in reactor, $cm.^3$
V_θ	tangential velocity component, dimensionless or cm./sec.
V_∞	terminal velocity of bubble, cm./sec.
x	mole fraction of solute in bulk gas
Y	mole ratio of oxygen to nitrogen in bulk gas
Y_ℓ	mole ratio of oxygen to nitrogen of bulk gas in equilibrium with bulk liquid
Z	film thickness, cm.

Greek Symbols

α	major axis of ellipse, cm.
β	minor axis of ellipse, cm.
γ	surface tension, dynes/cm.
δ	solubility parameter
θ	polar angle, radian
λ	volume fraction
μ	viscosity, centipoise
ρ	density, gm./c.c.

σ	associative parameter of solvent
ϕ	enhancement factor
ψ	stream function

Superscript

*	with chemical reaction

Subscripts

AcH	acetaldehyde
CoAc	cobaltous acetate
EtAc	ethyl acetate
IN	inlet stream
Mix	mixture of acetaldehyde and ethyl acetate
O_2	oxygen
OUT	outlet stream
PA	peracetic acid

TABLE OF CONTENTS

APPENDIX

FIGURE INDEX

Main Body

Appendix

TABLE INDEX

Main Body

Appendix

1. INTRODUCTION

Gas absorption is involved in chemical processes such as oxidation and separation. Very often bubble reactors are selected for these processes. A single-nozzle bubble reactor was used in this study of oxidation of acetaldehyde. There are several advantages for choosing the present apparatus. Firstly, the velocity distribution around a gas bubble rising in a liquid under the influence of gravity and other external forces may be described mathematically. This allows the solution of equations of changes for the gas bubble. In this study, only gravitational force was considered. The Sherwood number associated with the gas bubble may therefore be predicted. Absorption data may then be investigated in terms of a more realistic theoretical model. Secondly, bubble reactors are widely used in many chemical processing industries due to the large interfacial areas that may be generated and their low cost. Though the commercial bubble reactors and the present apparatus differ greatly in size and capacity, it is believed that the fundamental absorption processes are essentially similar.

The oxidation of acetaldehyde catalyzed by cobaltous acetate is chosen for this study because the products of the reaction, peracetic acid and acetic anhydride, may be of commercial interest if they can be produced at a low cost.

The influence of chemical reaction on gas absorption may be characterized by the enhancement factor ϕ, which is defined as K_L^*/K_L. The above reaction was studied in a simple stirred cell (35) under various

operating conditions and found that Φ was strongly dependent on catalyst concentration. However, theoretical study (36) indicated that Φ varies significantly with changes in velocity distribution. The results of the present investigation show that Φ is independent of the catalyst concentration. The absorption data agree with those predicted by theory (36).

2. LITERATURE REVIEW

2.1 Bubble Mechanics

Process equipment involving bubbling motion in liquids ~~are~~ is used in chemical, food and ore concentration industries. In order to predict the efficiency of such equipment, the fundamentals of bubble motion must be understood. Jackson (14) listed the following principal factors which influence the bubble diameters in his review article on the formation and coalescence of drops and bubbles in liquids:

"(1) Orifice diameter

(2) Volumetric gas flow rate through the orifice

(3) Density and viscosity of gas

(4) Density and viscosity of liquid

(5) Height of liquid above the orifice

(6) Surface tension

(7) Pressure drop across the orifice

(8) Volume of the gas chamber upstream of the orifice

(9) The velocity of sound in the gas

(10) Wetting properties of the materials of the orifice."

Most investigators (1, 2, 3, 4, 5, 6) concentrated their work on the physical phenomenon of mass transfer using an air-water system. Others (7, 8) worked with various systems where chemical reactions were present.

2.1.1 Bubble Shape and Size

The shape of the bubbles is a function of bubble velocity of rise,

gas flow rate, and physical properties of gases and liquids in the system. The shapes of bubbles were classified by Siemes and Gunther (9) according to bubble volume, by Datta et al. (10) according to bubble diameter, by Rosenberg (11) according to Reynolds Numbers. Table A summarizes their findings.

TABLE A CLASSIFICATION OF BUBBLES

	Spherical	Ellipsoidal	Flat Bottom (unstable)
Siemes and Gunther (9)	V_B < 0.05 c.c.	0.05 < V_B < .78 c.c.	V_B > .78 c.c.
Datta et al. (10)	d < 0.04 cm.	0.04 < d < .4 cm.	d > .4 cm.
Rosenberg (11)	N_{Re} < 400	400 < N_{Re} < 1100 varying geometric proportion 1100 Re 5000 constant geometric proportion.	N_{Re} > 5000

2.1.2 Bubble Velocity of Rise

Datta et al. (10) plotted terminal velocity versus bubble radius obtained by many workers for single bubbles and found that there was no consistent relationship. It was suggested that the variation might be due to temperature, wall effect, and accuracy of bubble size and velocity measurements. The same workers also collected data relating terminal velocity and bubble radius obtained by many investigators using air-water

systems, and showed the best curve drawn through these data.

The curve shown in Figure 1 was divided into three regions:

I. Streamline region, where the bubbles were fairly spherical and not oscillating, rising with straight line path,

II. Intermediate region, where the bubbles were ellipsoidal and flat, rising with zig-zag path, and

III. Turbulent region, where bubbles were deformed, and the path of rise was irregular.

There is little information about velocity of rise for a series of bubbles. Van Krevelen and Hoftijzer (1) noted that the ascending velocity of chain-like bubbles was different from that of separate bubbles. Haberman and Morton (2) found in an air-mineral oil system, that the bubble velocity increased 9% and 39% for bubbles of equivalent diameter 0.17 cm., rising 7.7 cm and 3.2 cm apart respectively. It is believed that the wake of the liquid caused the higher velocity of rise.

2.1.3 Motion of Rising Bubbles

Haberman and Morton (2) observed in their experiments that the rising bubbles displayed three types of motions: (i) rectilinear motion, (ii) motion in a helical path and (iii) rectilinear motion with rocking. The motion of the spherical bubbles was either rectilinear or helical, the ellipsoidal and flat-bottomed bubbles could have all three types of motions. The above authors (2) related the bubble motions with Reynolds Numbers:

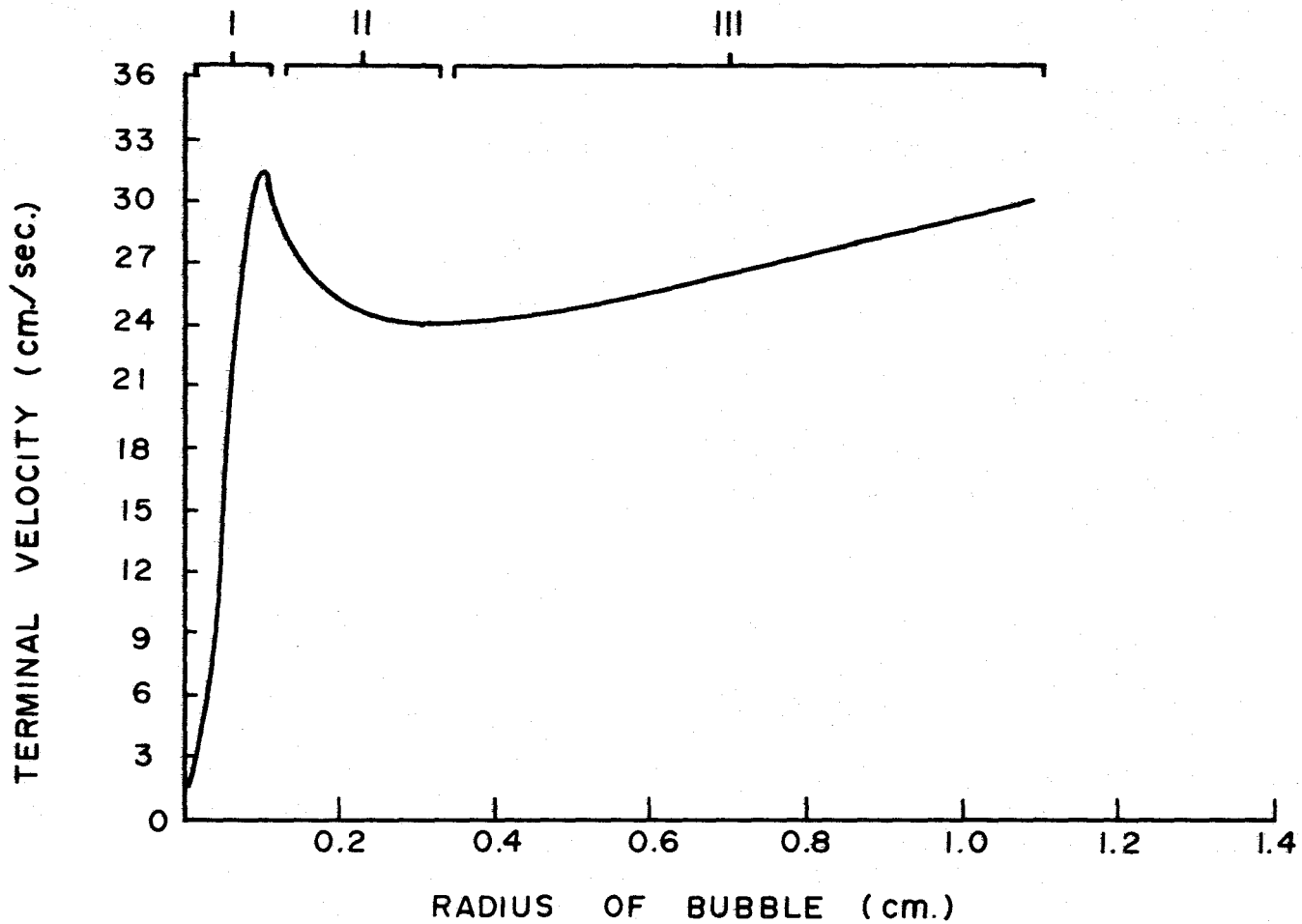

FIGURE 1 $V_\infty - R_b$ RELATION, AVERAGING THE RESULTS OBTAINED BY DIFFERENT AUTHORS

$N_{Re} < 300$	Rectilinear
$300 < N_{Re} < 3000$	Various degree of spiraling
$N_{Re} < 3000$	Rectilinear with rocking

Similar phenomena were observed by Datta et al. (10) who classified the bubble motion according to radius into three regions as shown in Figure 1.

2.1.4 Formation of Bubbles

(i) Formation of Separate Bubbles

Bubbles are formed as gas passes through a nozzle located underneath a column of liquid. Leibson et al. (6) gave an account of the mechanics of a single bubble formation. At the beginning of the process, the viscous drag force acting on the top surface of the nozzle accelerated the surrounding liquid away from the opening. As the bubble grew, the pressure upstream from the nozzle decreased, thus decreasing the bubble growth rate. However, the continuous flow of gas caused the upstream pressure to rise again and accelerated the bubble growth. During all these times, the liquid flowed inwards at the level of the nozzle, and the bubble was detached by a combination of the buoyancy force and the motion of the liquid flowing towards the nozzle. The pressure change upstream from the nozzle during the bubble formation period caused fluctuation of the rate of bubble formation. For low gas flow rates, Turner (12) found that the pressure change upstream from the nozzle did not affect the rate of bubble formation if the volume of the air chamber upstream from the nozzle was more than 10^4 times the volume of an individual bubble. Other workers found definite effects of the volume of such air chamber on bubble formation rate. Mahoney and Wenzel (13)

suggested that the air chambers above the liquid surface and below the nozzle influenced the bubble frequency and air flow rate. They also proposed a relationship which predicted sets of upper and lower chamber volumes to give the same bubble frequency and air flow rate.

If complete wetting of the nozzle and spherical shape bubbles were assumed, the bubble was released when the buoyancy force would be balanced with the force which held the bubble at the nozzle.

$$\frac{1}{6} \pi d^3 \Delta \rho g = \pi d_o \gamma \qquad (1)$$

Equation (1) shows that the bubble diameter is independent of the gas flow rate. Van Krevelen and Hoftijzer (1) analysed data of other workers and concluded that such a relationship only held below certain values of gas flow rate, called critical flow rates, above which, the bubble diameter increases with gas flow rate.

(ii) Formation of Bubbles in Series

As the gas flow rate increased for a given nozzle size, the bubble diameter would remain constant. If bubbles of a given diameter were assumed to have a particular velocity of rise, the distance between two successive bubbles would be inversely proportional to bubble frequency. However, the distance between succeeding bubbles could not be smaller than the bubble diameter. Therefore, above the critical gas flow rate, the gas must be transported by larger bubbles. Van Krevelen and Hoftijzer (1) showed the relationship between Ex ($\frac{gd\Delta\rho}{v_r \rho}$ expansion group) and Re and suggested that there were two regions where chain-like bubbles took place:

(i) Streamline region, where the relationships between Ex and N_{Re} for gas bubbles (both separated or chain-like) were the same as for solid spheres.

(ii) Turbulent region, where Ex was independent of N_{Re} for chain-like bubbles.

2.1.5 Bubble Frequency

At low gas flow rate, the bubble diameter remains reasonably constant, and increased gas flow rate increases the frequency of bubble formation. At higher gas flow rate, the bubble frequency remains relatively constant, and the diameters of the bubbles increase. At still higher gas flows, the bubbles produced will not have uniform sizes (1, 14)

2.1.6 Internal Circulation of Bubbles

As the bubble rises in the liquid, the viscous drag of the liquid causes circulation of gas inside the bubble, sending a regular current of gas up the central axis and down the sides of the bubble. This phenomenon was predicted by Hadamand (15) and Rybczynski (16), and was observed by many workers (2, 17, 18) in the field of mass transfer from bubbles and drops. The internal circulation of the bubbles would decrease if surfactants were present in the liquid (2, 17).

2.2 Mass Transfer

Many chemical processes involve the transfer of materials from one phase to another, such as the drying of solids and the recovery of valuable and nuisance gases by absorption, extraction and oxidation processes. This transport phenomenon may be expressed qualitatively by stating that the rate of mass transfer per unit area is proportional to the driving force or

$$N_A = k \text{ (driving force)} \qquad (2)$$

where k is the proportionality constant, the mass transfer coefficient. In a gas-liquid system, equation (2) may be expressed as

$$N_A = k_L (C_i - C) \tag{3}$$

if mass transfer is controlled by liquid phase resistance, and

$$N_A = k_G(p_i - p) \tag{4}$$

if mass transfer is controlled by gas phase resistance.

2.2.1 Film Theory

Whitman (19) was one of the first to suggest to chemical engineers an analysis of mass transfer rate based on the existence of two stagnant films, one on each side of the interface. For steady-state mass transfer in a gas-liquid system, all the solute diffusing from the gas phase to the interface must diffuse at the same rate from the interface to the bulk of the liquid. Therefore, the rate of mass transfer per unit area may be expressed as:

$$N_A = k_G (p - p_i) = k_L (C_i - C) \tag{5}$$

Usually, p_i and C_i are unknown, and equation (4) may be expressed as:

$$N_A = K_G(p - p_e) = K_L(C_s - C) \tag{6}$$

where p_e is the partial pressure of solute over a solution having the composition of the main stream composition C and C_s is the concentration of a solution in equilibrium with the solute partial pressure p. K_L and K_G are overall liquid phase and gas phase mass-transfer coefficients respectively. At steady-state, equation (6) may be written as

$$N_A = \frac{DP}{RTZ\ p_{BM}} (p_e - p)$$

$$= \frac{D}{Z} (C_s - C) \tag{7}$$

Whitman (19) showed the relationships between the gas and liquid phase mass transfer coefficients applying Henry's law relationship to the partial pressure of the gas and the saturation of the liquid.

$$\frac{1}{K_G} = \frac{1}{k_G} + \frac{H}{k_L} \tag{8}$$

$$\frac{1}{K_L} = \frac{1}{k_L} + \frac{1}{Hk_G} \tag{9}$$

Thus the overall mass-transfer coefficients resembled the overall electrical resistance where the individual resistances were placed in series.

Van Krevelen and Hoftijzer (21) studied slow second order chemical reaction using this film theory.

2.2.2 Penetration Theory

Whitman's two-film theory assumes that the hold-up of solute in the film is negligible and that, therefore, steady-state is reached instantaneously. Higbie's (22) penetration theory on the other hand, accounts for the transient period leading to steady state. Using this concept Higbie proposed an equation to evaluate physical mass-transfer coefficients for transfer into a semi-infinite medium.

$$k_L = 2\sqrt{\frac{D}{\pi t_e}} \tag{10}$$

where k_L is a mass-transfer coefficient averaged over the life of the fluid element, t_e.

Danckwerts (23) extended the penetration theory to take into consideration that the exposed liquid surface was continuously being randomly replaced by turbulent motion in the liquid phase. Toor and Marchello (24) considered a finite depth of liquid element brought to the surface by turbulence in the liquid phase and proposed that the film theory and penetration theory were extremes of the general model. Brian et al. (25, 26) studied experimentally and numerically gas absorption accompanied by 2nd order chemical reaction. Their results were interpreted in the light of both film theory and penetration theory. Brian (27) also solved penetration-theory equations for gas absorption accompanied by an irreversible chemical reaction of general order. Sherwood and Pigford (28) summarized Hatta's and Higbie's concepts and derived equations for simultaneous absorption and chemical reactions for the following cases:

(A) Stagnant film of finite thickness
  (i) rapid 2nd order irreversible reaction
  (ii) slow 1st order reaction.

(B) Unsteady-state absorption in stagnant liquid
  (i) slow 1st order reaction
  (ii) rapid 2nd order irreversible reaction.

2.3 Reaction Kinetics

The present study concerns the oxidation of acetaldehyde by air. The reaction leads to a number of products depending on the temperature of oxidation and the catalyst used. In addition to acetic acid, peracetic

acid, if it could be produced cheaply from this reaction has considerable industrial potential as an epoxidizing agent. Phillips et al. (29) summarized the various reaction routes of oxidation of acetaldehyde at low temperature as follows

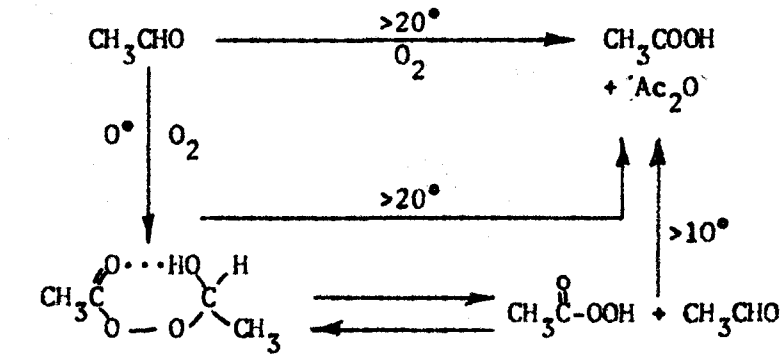

Acetaldehyde Monoperacetate
AMP

Bawn and Williamson (30) postulated that oxidation of acetaldehyde with cobaltous acetate as catalyst was a chain reaction. The following mechanism was proposed as result of their investigation at 25°C:

Initiation

$$Co^{+++} + CH_3COOOH \longrightarrow Co^{++} + H^+ + CH_3COO^{\cdot}$$

$$Co^{++} + CH_3COOOH \longrightarrow Co^{+++} + CH_3COO^{\cdot} + OH$$

$$CH_3COO^{\cdot} + CH_3CHO \longrightarrow CH_3COOH + CH_3CO^{\cdot}$$

Propagation

$$CH_3CO^{\cdot} + O_2 \longrightarrow CH_3COOO^{\cdot}$$

$$CH_3COOO^{\cdot} + CH_3CHO \longrightarrow CH_3COOOH + CH_3CO^{\cdot}$$

Termination

$$CH_3COOO^{\cdot} + CH_3COOOH \longrightarrow \text{inactive products}$$

$$2CH_3COOO^{\cdot} \longrightarrow \text{inactive products.}$$

and the rate equation was expressed as

$$\frac{-dC_{O_2}}{dt} = k'' C_{AcH} C_{CoAc} \qquad (11)$$

Bolland et al. (31, 32) studied oxidation of olefins and proposed a mechanism which Twigg (33) believed might be applied to oxidation of acetaldehyde. The rate equation for oxidation of acetaldehyde according to Bolland's mechanism might be simplified as:

$$\frac{-dC_{O_2}}{dt} = k''' C_{PA}^{1/2} C_{CoAc}^{1/2} C_{AcH} \qquad (12)$$

Carpenter (34) investigated the same system at 56°C and concluded that the main reactions were:

$$\text{Aeetaldehyde} \longrightarrow \text{acetaldehyde monoperacetate (AMP)}$$

$$\xrightarrow[\text{CuAc}]{\text{CoAc}} \text{Acetic anhydride} \xrightarrow{\text{hydrolysis}} \text{acetic acid.}$$

The mechanism of the catalytic oxidation of acetaldehyde was expressed in seven steps:

1. $CH_3CHO + O_2 \longrightarrow CH_3COOOH$
2. $CH_3COOOH + CH_3CHO \longrightarrow AMP$
3. $AMP \longrightarrow (CH_3CO)_2O + H_2O$
4. $AMP \longrightarrow 2CH_3COOH$
5. $(CH_3CO)_2O + H_2O \longrightarrow 2CH_3COOH$
6. $(CH_3CO)_2O + CH_3COOOH \longrightarrow (CH_3CO)_2O_2 + CH_3COOH$
7. $(CH_3CO)_2O_2 + H_2O \longrightarrow CH_3COOOH + CH_3COOH$

Pang (35) studied the catalytic oxidation of acetaldehyde in a stirred apparatus using cobaltous acetate as catalyst. His investigation included the effects of acetaldehyde concentration, catalyst concentration,

partial pressure of oxygen and temperature on the rate of absorption. The mathematical models based on Bolland's and Bawn's reaction mechanisms predicted the rate of absorption with moderate success. The difficulties encountered in such an attempt were in part due to the undefined hydrodynamics of the stirred apparatus and the unknown physical properties and stability of the reactants and products.

3. SCOPE

A single nozzle bubble reactor was used to study the rate of oxygen transfer in an oxidation reaction. The reaction chosen was air oxidation of acetaldehyde catalyzed by cobaltous acetate. The parameters studied included temperature, catalyst concentration, column height and air flow rate.

The experimental results were used to test the mathematical model based on Houghton's work (36) to predict the absorption rate from a single gas bubble.

4. THEORY

4.1 Mass Transfer in a Bubble Column

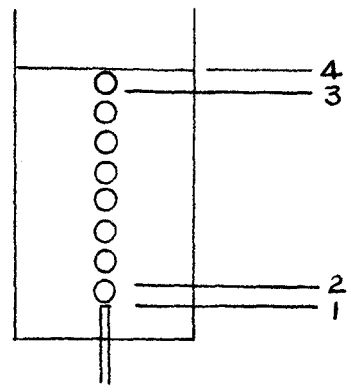

FIGURE 2 SCHEMATIC REPRESENTATION OF A BUBBLE COLUMN

From a
A material balance on a differential section of the bubble column, the rate of mass transfer may be expressed as

$$- G_N dY = K_G a \, (Y - Y_\ell) \, dh \qquad (13)$$

where

G_N = nitrogen flow rate, g. mole/sec.

Y = mole ratio of oxygen to nitrogen in bulk gas

Y_ℓ = mole ratio of oxygen to nitrogen of bulk gas in equilibrium with bulk liquid

K_G = overall gas phase mass-transfer coefficient, moles O_2/cm^2 sec.

a = bubble surface area per unit column height, cm^2/cm.

h = column height, cm.

Equation (13) may be rearranged as

$$\frac{dY}{Y - Y_\ell} = \frac{-K_G a}{G_N} dh \qquad (14)$$

and integrated to give

$$\ln \frac{(Y - Y_\ell)_{IN}}{(Y - Y_\ell)_{OUT}} = \frac{K_G a}{G_N} h \qquad (15)$$

The term on the left hand side is referred to as the number of transfer units (N.T.U.). A plot of N.T.U. vs. h gives a straight line with slope equal to $K_G a/G_N$.

It may be assumed that the amount of disolved oxygen present in the bulk of the liquid is negligible compared to the saturation of the oxygen in the liquid. Equation (15) becomes

$$\ln \frac{Y_{IN}}{Y_{OUT}} = \frac{K_G a}{G_N} h \qquad (16)$$

For a particular gas flow rate, the oxygen content of the inlet and outlet gas streams at various column heights may be measured. Therefore $K_G a$ may be obtained from N.T.U. vs. h plot.

Equation (8) relates the overall gas-phase mass-transfer coefficient to the individual gas and liquid mass-transfer coefficients. For a slightly soluble gas, the resistance to mass transfer in the gas phase may be negligible, and equation (8) becomes

$$k_L = HK_G \qquad (17)$$

where H = Henry's law constant.

4.2 End Effects in a Bubble Column

The rate of mass transfer during the periods of bubble formation

at the nozzle and bubble break-up at the top of the column may be different from that during the steady rise period. This phenomenon may be considered as an end effect.

Region 1-2 in Figure 2 represents the formation end effect and region 3-4 represents the break-up end effect. It is not possible in this study to separate these effects. However, it can be shown that mass transfer coefficients for the rise period calculated from equation (16) are free of such effects.

If the bubble column is divided into regions as shown in Figure 2, equation (14) may be written as

$$\int_{Y_1}^{Y_4} \frac{dY}{Y - Y_\ell} = \int_{Y_1}^{Y_2} \frac{dY}{Y - Y_\ell} + \int_{Y_2}^{Y_3} \frac{dY}{Y - Y_\ell} + \int_{Y_3}^{Y_4} \frac{dY}{Y - Y_\ell} = -\int_{o}^{h} \frac{K_G a}{G_N} dh \tag{18}$$

Therefore

$$\ell n \frac{Y_4 - Y_\ell}{Y_1 - Y_\ell} = \underbrace{\ell n \frac{Y_2 - Y_\ell}{Y_1 - Y_\ell}}_{\text{N.T.U. during bubble formation}} + \underbrace{\ell n \frac{Y_3 - Y_\ell}{Y_2 - Y_\ell}}_{\text{N.T.U. during steady rise period}} + \underbrace{\ell n \frac{Y_4 - Y_\ell}{Y_3 - Y_\ell}}_{\text{N.T.U. during bubble break-up}} \tag{19}$$

The following definitions are used to show the first and last terms on the R.H.S. of equation (19) are independent of column height.

$$E_B = \frac{Y_1 - Y_2}{Y_1 - Y_\ell} \tag{20}$$

$$E_T = \frac{Y_3 - Y_4}{Y_3 - Y_\ell} \tag{21}$$

$$1 - E_B = \frac{Y_1 - Y_\ell - Y_1 + Y_2}{Y_1 - Y_\ell} = \frac{Y_2 - Y_\ell}{Y_1 - Y_\ell} \tag{22}$$

$$1 - E_T = \frac{Y_3 - Y_\ell - Y_3 + Y_4}{Y_3 - Y_\ell} = \frac{Y_4 - Y_\ell}{Y_3 - Y_\ell} \qquad (23)$$

Substituting equations (22) and (23) into equation (19)

$$\ell n \frac{Y_4 - Y_\ell}{Y_1 - Y_\ell} = \ell n \frac{Y_3 - Y_\ell}{Y_2 - Y_\ell} + \ell n\,[(1 - E_B)(1 - E_T)] \qquad (24)$$

The last term in equation (24) is independent of column height by definition.

4.3 Mass Transfer from a Single Gas Bubble

Houghton et al. (36) obtained numerical solutions of mass transfer with[a] first order irreversible chemical reaction from a single gas bubble

$$V_r \frac{\partial C}{\partial r} + \frac{V_\theta}{r} \frac{\partial C}{\partial \theta} = \frac{2}{Pe} \left[\frac{\partial^2 C}{\partial r^2} + \frac{2}{r} \frac{\partial C}{\partial r} + \frac{\cot\theta}{r^2} \frac{\partial C}{\partial \theta} + \frac{1}{r^2} \frac{\partial^2 C}{\partial \theta^2} + k_1 C \right] \qquad (25)$$

Equation (25) is expressed in dimensionless form and is derived from mass balance on a spherical volume element on the gas bubble with the following assumptions:

(1) steady-state condition

(2) incompressible flow

(3) axisymmetric flow

(4) constant molecular diffusion coefficient

The boundary conditions are:

$$\begin{aligned} C &= 1 \quad \text{at} \quad r = 1 \\ C &= 0 \quad \text{at} \quad r = \infty \\ \frac{\partial C}{\partial \theta} &= 0 \quad \text{at} \quad \theta = 0, \pi \end{aligned} \qquad (26)$$

The velocity profile for potential flow is

$$V_\theta = \left(1 + \frac{1}{2 r^3}\right) \sin\theta \qquad (27)$$

$$V_r = -(1 - \frac{1}{r^3}) \cos\theta \tag{28}$$

The numerical solution gives concentration as a function of r and θ, and the local mass transfer coefficients can be calculated from

$$k_L = \frac{-D}{C_s} \left(\frac{\partial C}{\partial r} \right)_{r=R_b} \tag{29}$$

or expressed in dimensionless form as:

$$N_{Sh} = -2\left(\frac{\partial C}{\partial r}\right)_{r=1} \tag{30}$$

4.4 Enhancement Factor

The effect of chemical reaction on mass transfer may be expressed as an enhancement factor, the definition of which is

$$\Phi = \frac{K_L^*}{K_L} \tag{31}$$

where K_L^* and K_L are the overall liquid phase mass transfer coefficients with and without chemical reaction respectively. Φ may also be expressed in terms of K_G^* and K_G if the gas phase resistance is considerable.

5. EXPERIMENTAL DETAILS

5.1 Description of Apparatus

Figure 3 is a schematic diagram of the continuous-flow bubble apparatus. The bubble column [1] consisted of a 5/8 in. I.D. glass tube, 26 in. long with three outlets [2] 5 in. apart enclosed in a glass cooling jacket [10]. A specially machined Teflon plug [3], having the air and liquid inlets, was fitted in a ground glass joint at the bottom of the column. The liquid reactant was put into a two-litre flask [9] which acted as a reservoir and was then pumped to the bottom of the column by means of a Beckman model 726 solution metering pump. The liquid was dispersed by a packing of glass beads before reaching the tip of the gas inlet. The filtered laboratory air was used in the experiments. A capillary flow meter [14] was used to measure air flow rate and an on-line soap-bubble meter [15] made from a 50 ml. burette provided instant check on the flow meter. The exit air passed through two dry ice-acetone cold traps [17] before reaching the sensor of the Beckman model 777 oxygen analyser [18].

5.2 Experimental Procedure

For each experimental run, fresh cobaltous acetate catalyst was prepared. At the beginning of the experiment, the oxygen analyser was calibrated with atmospheric air. The apparatus was purged with nitrogen before the reactants were introduced into the reservoir which was blanketed with nitrogen throughout the experiment. At the same time, air was admitted into the apparatus through the capillary flow meter. The

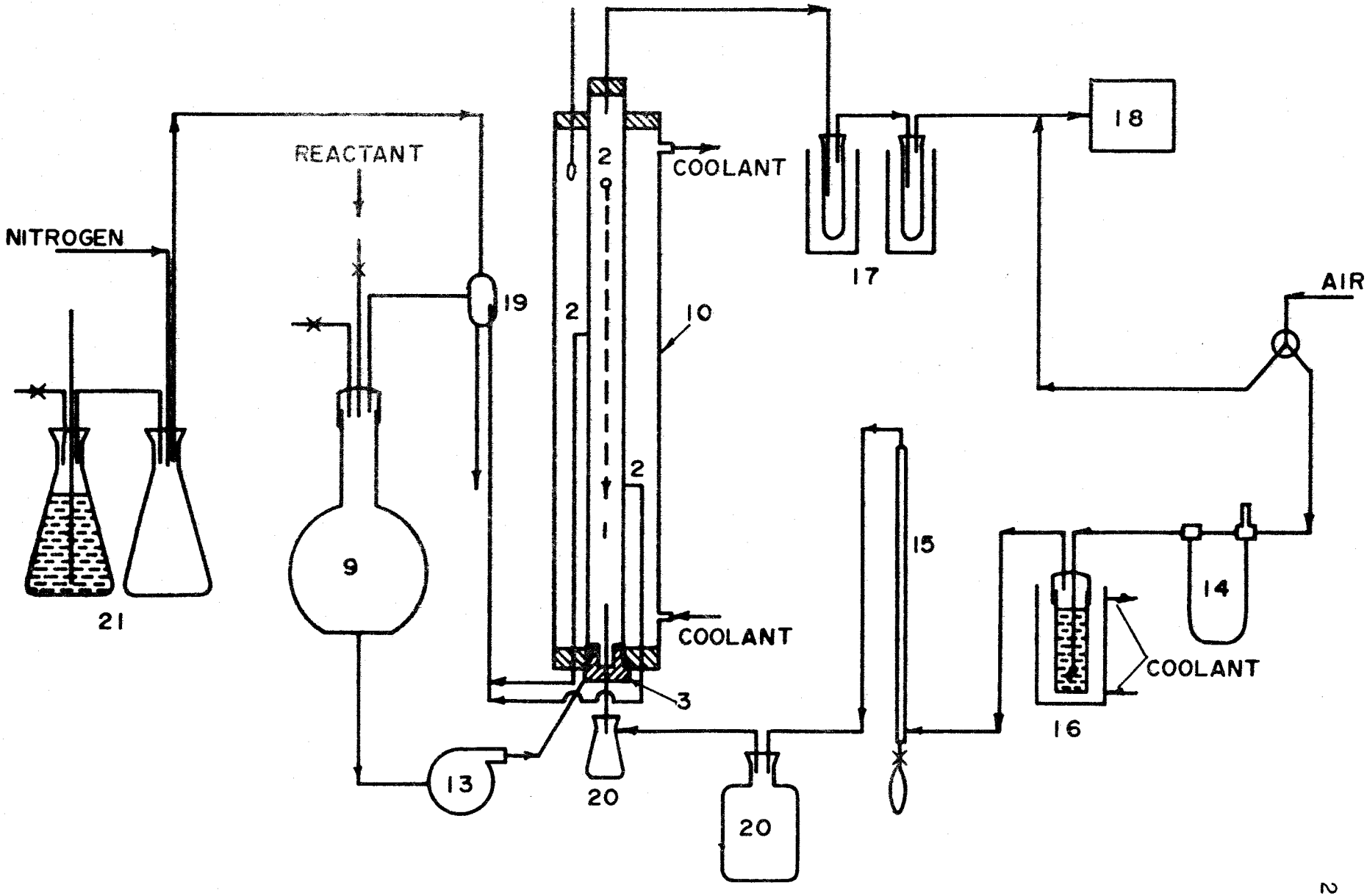

21a

FIGURE 3 SCHEMATIC DIAGRAM OF CONTINUOUS FLOW BUBBLE COLUMN

height of the column was adjusted to a desirable value by raising and lowering the levelling device. The apparatus was allowed to operate until the oxygen analyser registered a constant reading, that is, when the absorption of oxygen in the bubble column reached a steady state. A 15 ml. liquid sample was then taken and analysed for peracetic acid, AMP, acetic acid and acetaldehyde.

A General Radio type 1531-A strobotac was used to measure the frequency of bubble generation.

Cine pictures and single frame pictures were taken with a Bolex 16 mm. cine camera and a Pentax 35 mm. camera respectively for various air flow rates. These pictures were used to analyse for ~~bubble~~ the velocity of bubble rise and shape.

6. EXPERIMENTAL RESULTS

The results obtained from the investigation may be categorized into the following sections.

6.1 Photographic Studies

Cine pictures and single frame pictures were taken to analyse the shapes and motion of the bubbles, the bubble velocity of rise and frequency of generation. Figure 4 is a typical photograph and shows that the bubbles are essentially ellipsoidal. At low gas flow rates the bubbles rise in a zig-zag path with helical motion. At higher gas flow rates, the bubbles rise in an irregular path with rocking motion. Appendix A-1 shows the detailed analysis of the photographic results to obtain bubble velocity of rise and frequency of generation; corrections for optical distortion are discussed in this appendix.

6.2 Mass Transfer

In this study of catalysed oxidation of acetaldehyde in ethyl acetate with a continuous flow bubble column, only one liquid flow-rate (3.3 c.c./min.) and one acetaldehyde concentration (5% by vol.) were used. The variables studied in this investigation included

3 temperatures	5,	10,	15	°C.
3 catalyst concentrations	2.8,	5.6,	11.2	ppm
3 column heights (approx.)	15,	27,	42	cm.
3 air flow rates (approx.)	10,	30,	50	c.c./min.

For each temperature and catalyst concentration the number of transfer units was plotted against column height with air flow rate as a parameter. The results of this investigation are summarized in Tables 1 to 4 and Figures 5 to 7. The experimental data were fitted with least square straight lines to obtain the slopes and the intercepts. The slope of the straight line is interpreted as $K_G a/G_N$ and its intercept is an indication of the end effects of the apparatus.

The physical mass-transfer coefficients were estimated using the Boussinesq equation

$$N_{Sh} = 1.13 \ (N_{Pe})^{0.5} \qquad (32)$$

The results are shown in Table 5. The variation of K_L with air flow rate is caused by the change in bubble diameters and the variation of K_L with temperature is caused by the change in diffusivities of oxygen in the mixture of acetaldehyde and ethyl acetate. The enhancement factors, Φ, at various temperature and air flow rates are summarized in Table 6.

6.3 Product Distribution

When steady-state was reached during each experimental run, 15 ml. of liquid sample was taken and analysed for peracetic acid, AMP, acetic acid and acetaldehyde. The analytical methods employed were identical to those described by Pang (35). The results of the analyses expressed in weight percent are shown in Tables 7 to 9.

6.4. Numerical Solutions

The Reynolds numbers of the bubbles obtained in this study were in the range of 800 to 1200, hence the velocity profile around the bubbles

might be approximated by potential flow (37). The numerical solution of mass transfer with first order chemical reaction from a single gas bubble proposed by Houghton et al. (36) was modified using velocity profiles for potential flow. The solutions gave the theoretically predicted Sherwood numbers. Table 10 shows the comparison of the predicted and experimental Sherwood numbers.

The effects of first order reaction rate constant on Sherwood numbers and enhancement factors were predicted by the numerical solutions. Table 11 summarizes the results.

(a) Air Flow Rate = 10 c.c./min.

(b) Air Flow Rate = 30 c.c./min.

(c) Air Flow Rate = 50 c.c./min.

FIGURE 4 TYPICAL SHAPES OF BUBBLES AT VARIOUS AIR FLOW RATES

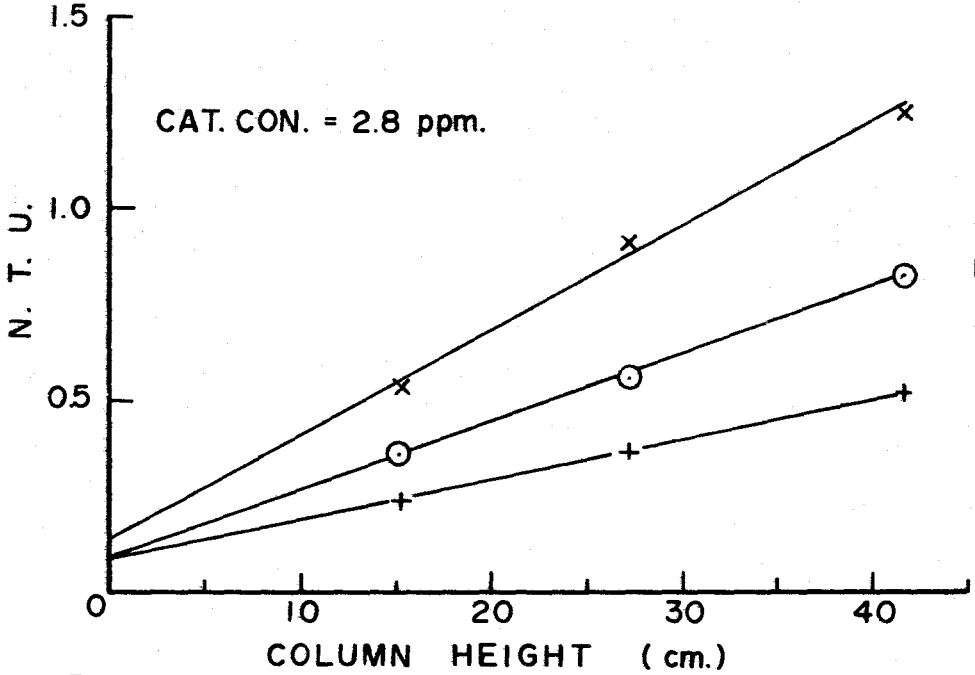

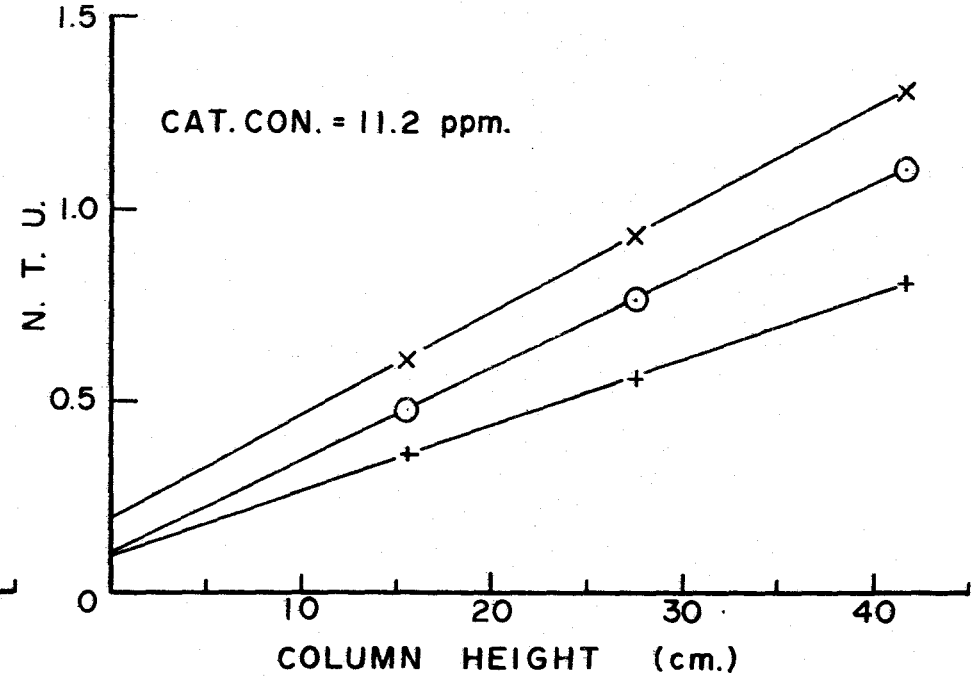

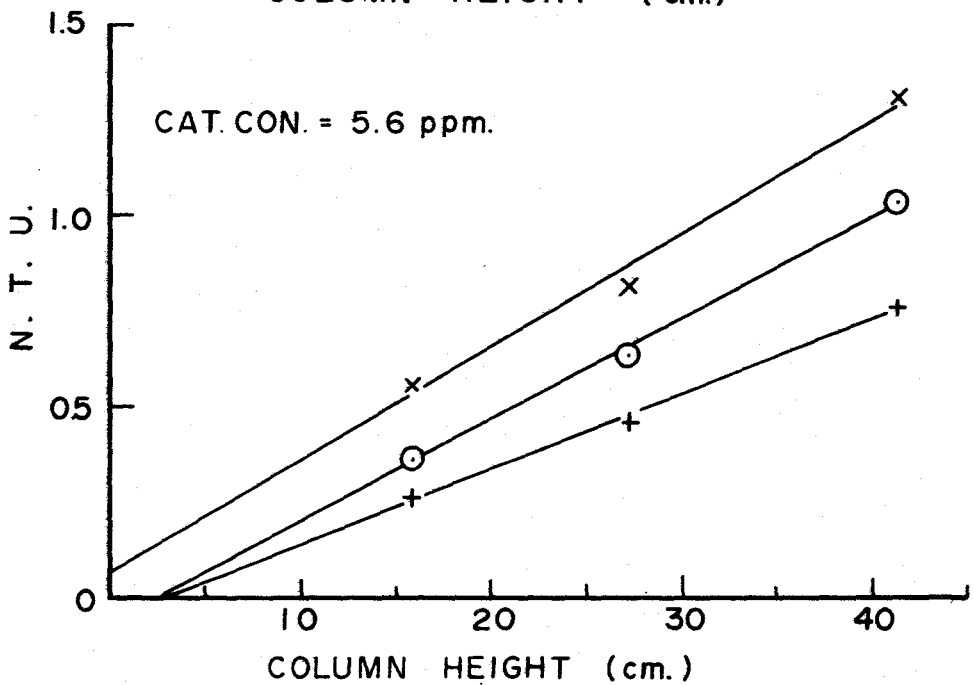

FIGURE 5 EXPERIMENTAL RESULTS AT 5° C

AIR FLOW RATE (c.c./min.)

×	10
⊙	30
+	50

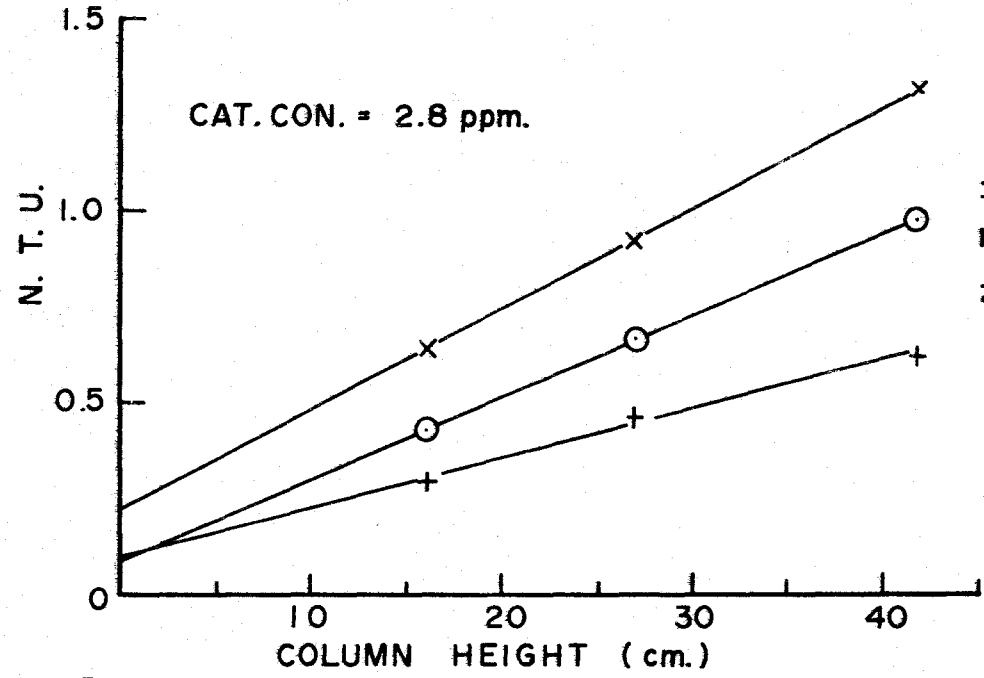

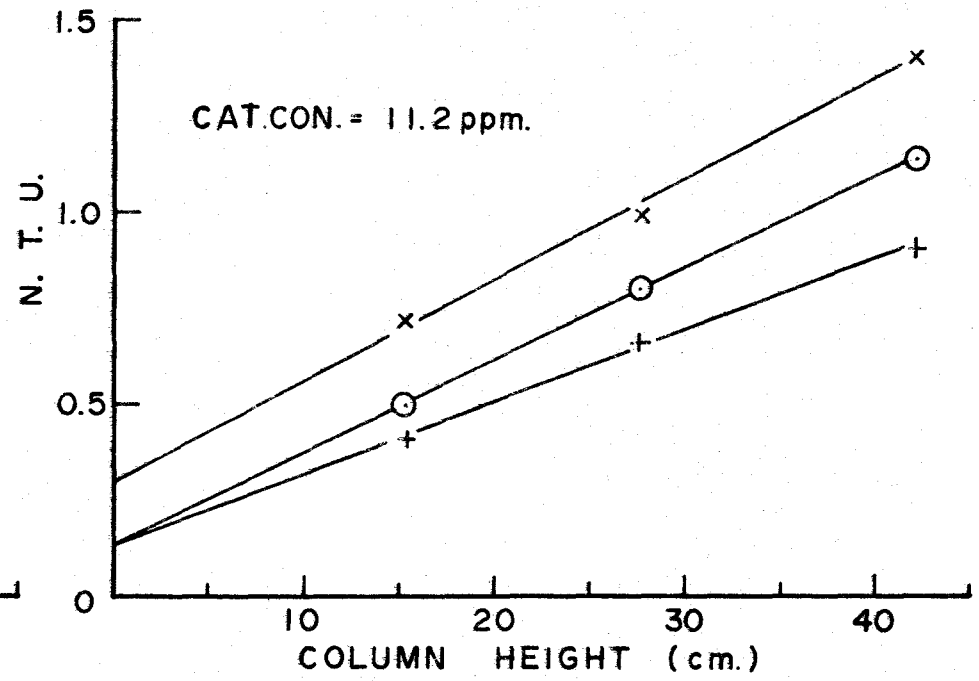

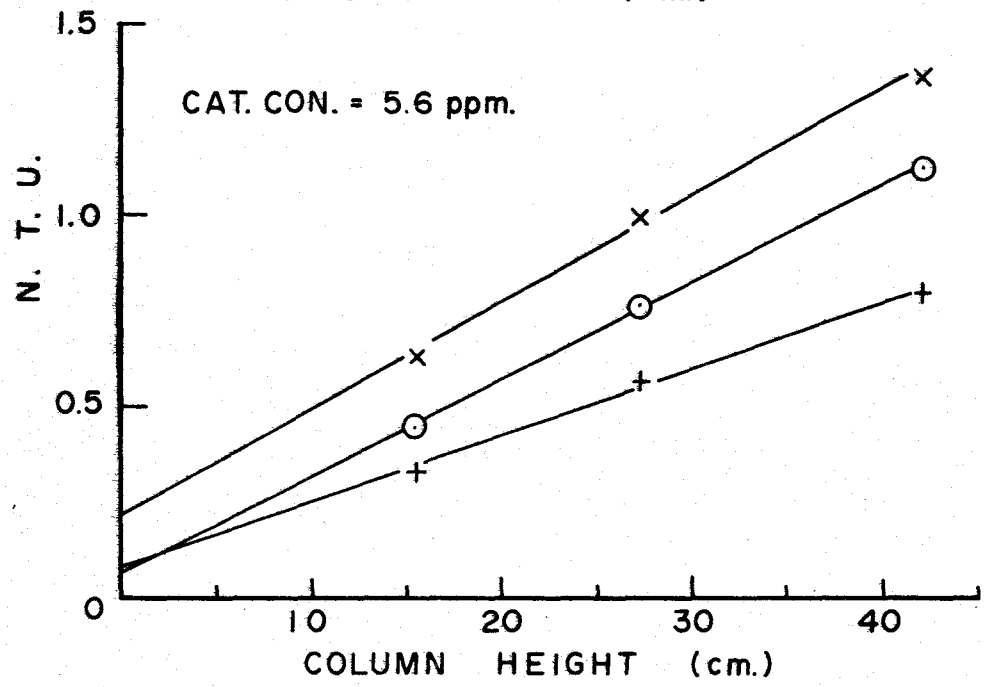

FIGURE 6 EXPERIMENTAL RESULTS AT 10° C

AIR FLOW RATE (c.c./min.)

× 10
⊙ 30
\+ 50

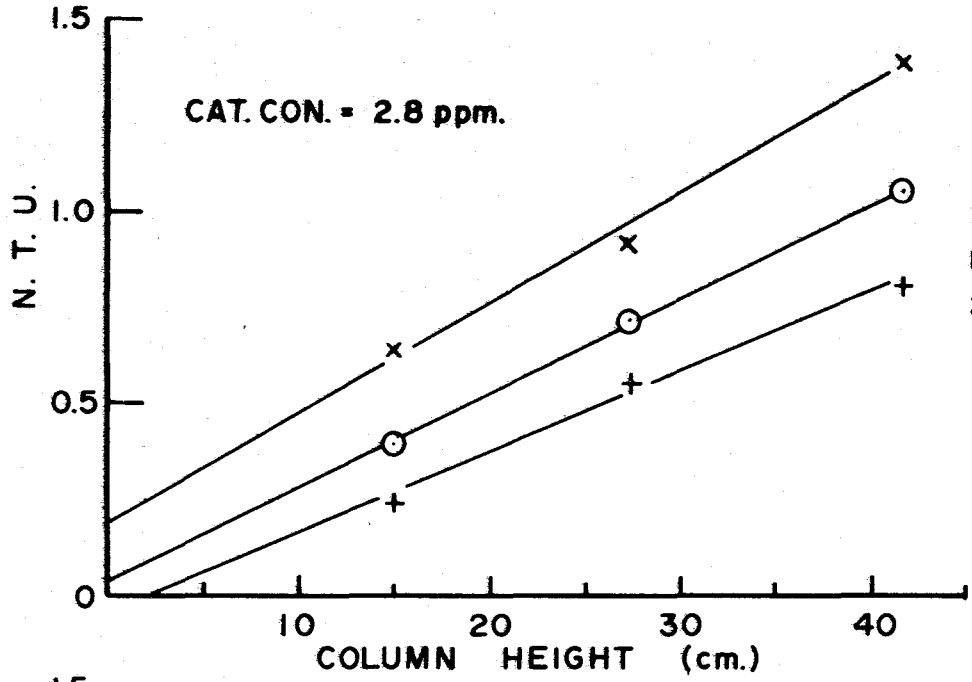

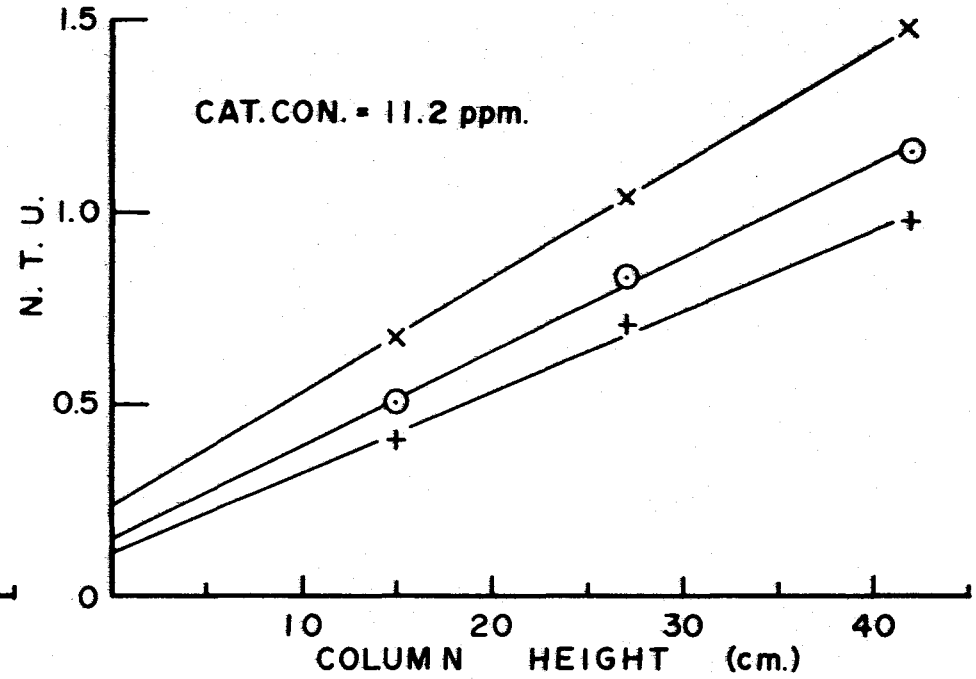

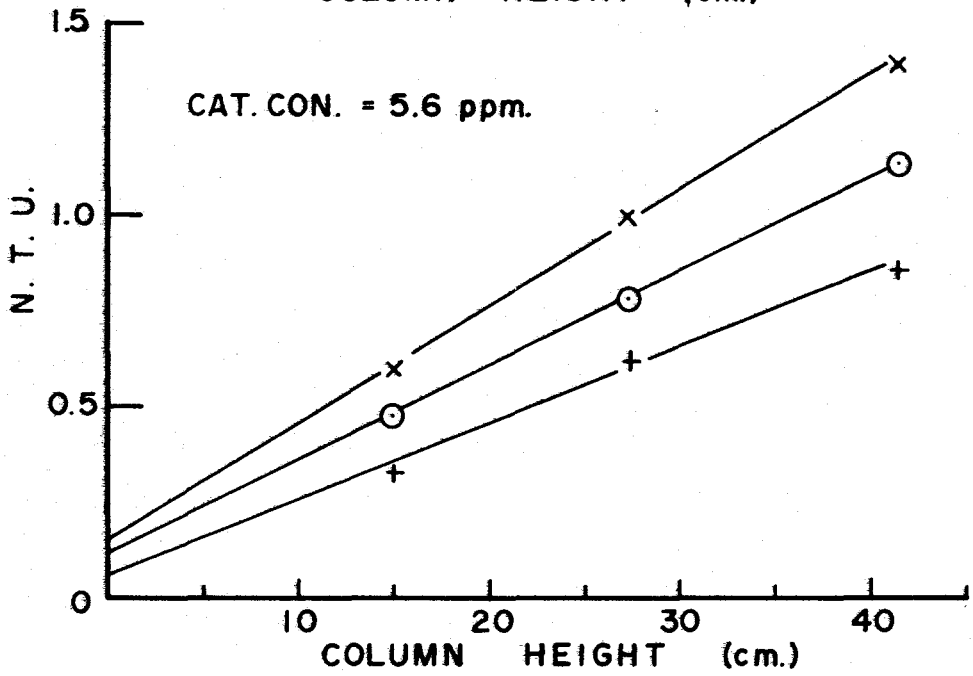

FIGURE 7 EXPERIMENTAL RESULTS AT 15°C

AIR FLOW RATE (c.c./min.)

× 10

⊙ 30

\+ 50

TABLE 1 EXPERIMENTAL RESULTS AT 5°C

Catalyst Concentration ppm	Column Height cm.	Air Flow Rate c.c./min.	N.T.U.
2.8	15.36	9.6	0.533
		29.5	0.364
		48.0	0.247
	27.25	10.3	0.909
		28.6	0.560
		48.5	0.356
	41.69	9.7	1.25
		30.2	0.82
		48.2	0.52
5.6	15.94	10.7	0.565
		30.5	0.372
		50.5	0.268
	27.38	10.1	0.818
		30.0	0.631
		48.5	0.457
	41.30	9.8	1.31
		29.4	1.04
		48.2	0.76
11.2	15.51	10.3	0.613
		29.9	0.476
		48.2	0.358
	27.60	9.6	0.93
		28.4	0.765
		48.8	0.56
	41.70	10.3	1.31
		29.4	1.10
		48.4	0.807

TABLE 2 EXPERIMENTAL RESULTS AT 10°C

Catalyst Concentration ppm	Column Height cm.	Air Flow Rate c.c./min.	N.T.U.
2.8	16.18	9.6	0.642
		31.2	0.425
		48.2	0.293
	27.0	10.2	0.92
		29.2	0.657
		49.1	0.457
	41.85	10.4	1.29
		28.8	0.97
		48.0	0.62
5.6	15.5	10.1	0.631
		30.0	0.445
		49.0	0.336
	27.31	10.1	0.99
		31.0	0.756
		48.4	0.565
	42.11	10.0	1.373
		28.2	1.12
		48.7	0.80
11.2	15.42	9.6	0.72
		30.2	0.495
		48.5	0.414
	27.63	10.2	1.01
		28.9	0.79
		49.5	0.641
	42.05	9.8	1.39
		29.3	1.13
		49.2	0.91

TABLE 3 EXPERIMENTAL RESULTS AT 15°C

Catalyst Concentration ppm	Column Height cm.	Air Flow Rate c.c./min.	N.T.U.
2.8	14.98	9.4	0.642
		29.9	0.399
		49.1	0.247
	27.45	9.3	0.924
		29.4	0.718
		48.4	0.560
	41.60	9.6	1.39
		28.9	1.05
		48.8	0.82
5.6	14.97	9.9	0.593
		27.1	0.476
		49.1	0.344
	27.33	10.2	0.990
		29.2	0.789
		49.2	0.620
	41.45	9.9	1.39
		28.3	1.13
		50.0	0.87
11.2	14.96	10.6	0.678
		29.9	0.507
		49.2	0.406
	27.06	10.1	1.04
		30.0	0.837
		47.7	0.708
	41.85	9.3	1.483
		30.3	1.160
		48.5	0.979

TABLE 4 MASS-TRANSFER COEFFICIENTS WITH CHEMICAL REACTION

Temp. °C	Catalyst Concentration ppm	Approx.. Air Flow Rate c.c./min	Intercept (End Effect) N.T.U.	Slope $\times 10^2$	$K_L^* \times 10^2$ cm/sec.
5	2.8	10	0.135	2.96	7.24
		30	0.094	2.64	5.07
		50	0.083	1.93	3.71
	5.6	10	0.063	2.71	8.00
		30	-0.063	1.73	7.77
		50	-0.051	1.04	6.93
	11.2	10	0.198	2.66	7.17
		30	0.103	2.40	7.00
		50	0.090	1.72	6.16
10	2.8	10	0.233	2.78	7.00
		30	0.083	2.53	6.54
		50	0.098	1.73	4.64
	5.6	10	0.211	2.53	7.69
		30	0.057	2.12	7.81
		50	0.077	1.27	6.42
	11.2	10	0.297	2.60	7.25
		30	0.131	2.38	6.74
		50	0.128	1.85	6.74
15	2.8	10	0.193	3.02	7.90
		30	0.039	2.46	7.48
		50	-0.045	1.97	7.92
	5.6	10	0.149	2.83	8.60
		30	0.111	2.44	7.54
		50	0.060	2.08	7.40
	11.2	10	0.230	2.99	8.36
		30	0.158	2.42	7.60
		50	0.105	2.12	8.03

TABLE 5 PHYSICAL MASS-TRANSFER COEFFICIENTS

Temp. °C	Approx. Air Flow Rate c.c./min.	N_{Sh}	$K_L \times 10^2$ cm./sec
5	10	331	7.2
	30	372	6.92
	50	401	6.51
10	10	314	7.37
	30	356	7.18
	50	395	6.97
15	10	306	7.75
	30	344	7.52
	50	370	7.04

TABLE 6 ENHANCEMENT FACTORS

Temp °C	Catalyst Concentration ppm	Approx. Air Flow Rate c.c./min	Φ
5	2.8	10	1.01
		30	0.73
		50	0.57
	5.6	10	1.11
		30	1.12
		50	1.07
	11.2	10	1.00
		30	1.01
		50	0.95
10	2.8	10	0.96
		30	0.91
		50	0.67
	5.6	10	1.04
		30	1.09
		50	0.92
	11.2	10	0.99
		30	0.94
		50	0.97
15	2.8	10	1.02
		30	1.00
		50	1.13
	5.6	10	1.11
		30	1.00
		50	1.05
	11.2	10	1.08
		30	1.01
		50	1.14

TABLE 7 PRODUCT DISTRIBUTION AT 5°C (wt.%)

Column Height cm.	Catalyst Concentration ppm	Air Flow Rate (Approx.) c.c./min	AcH Initial	P.A.	AMP	AcOH	AcH Final
15.36	2.8	10	4.41	.08	.106	.055	4.13
		30		.157	.085	.102	3.99
		50		.168	.017	.264	3.90
15.94	5.6	10	4.45	.034	.115	.159	3.99
		30		.080	.082	.266	3.82
		50		.10	.072	.272	3.75
15.51	11.2	10	4.45	.051	.116	.184	4.00
		30		.147	.111	.277	3.83
		50		.195	.072	.340	3.72
27.25	2.8	10	4.42	.113	.109	.019	4.12
		30		.241	.027	.207	3.92
		50		.274	.040	.198	3.86
27.38	5.6	10	4.41	.093	.103	.126	3.58
		30		.204	.051	.327	3.62
		50		.278	0	.402	3.50
27.60	11.2	10	4.42	.067	.123	.197	3.75
		30		.186	.067	.337	3.54
		50		.304	.030	.370	3.54
41.69	2.8	10	4.40	.122	.154	0	3.88
		30		.302	.031	.205	3.67
		50		.359	.021	.172	3.67
41.30	5.6	10	4.38	.099	.067	.170	3.86
		30		.268	.030	.297	3.80
		50		.387	0	.488	3.56
41.7	11.2	10	4.37	.077	.161	.131	3.65
		30		.252	.063	.375	3.55
		50		.391	0	.508	3.45

TABLE 8 PRODUCT DISTRIBUTION AT 10°C (wt. %)

Column Height cm.	Catalyst Concentration ppm	Air Flow Rate (Approx.) c.c./min	AcH Initial	P.A.	AMP	AcOH	AcH Final
16.18	2.8	10	4.46	.067	.140	0	3.34
		30		.178	.075	.155	3.17
		50		.229	.059	.170	2.93
15.5	5.6	10	4.41	.057	.092	.120	3.77
		30		.160	.084	.101	3.63
		50		.208	.086	.149	3.53
18.65	11.2	10	4.22	.063	.103	.192	3.27
		30		.181	.074	.379	2.72
		50		.249	.024	.427	3.14
27.0	2.8	10	4.26	.101	.097	.059	4.02
		30		.261	.039	.186	3.87
		50		.339	.023	.273	3.78
27.31	5.6	10	4.39	.074	.122	.109	4.02
		30		.252	.061	.209	3.77
		50		.342	.027	.249	3.63
27.16	11.2	10	4.07	.066	.108	.144	3.86
		30		.219	.041	.374	3.70
		50		.327	.012	.504	3.56
41.85	2.8	10	4.31	.124	.099	.043	3.73
		30		.331	0	.269	3.59
		50		.477	0	.269	3.33
42.11	5.6	10	4.45	.089	.119	.034	3.82
		30		.276	.023	.217	3.61
		50		.418	.023	.319	3.31
41.34	11.2	10	4.22	.076	.137	.097	4.06
		30		.266	.053	.296	3.77
		50		.414	.01	.390	3.80

TABLE 9 PRODUCT DISTRIBUTION AT 15°C (wt. %)

Column Height cm.	Catalyst Concentration ppm	Air Flow Rate (Approx.) c.c./min	AcH Initial	P.A.	AMP	AcOH	AcH Final
14.96	2.8	10	4.36	.090	.129	0	4.29
		30		.192	.069	.10	4.07
		50		.227	.056	.032	3.97
14.97	5.6	10	4.27	.062	.097	.067	4.02
		30		.151	.063	.164	3.96
		50		.228	.012	.225	3.76
14.96	11.2	10	4.29	.050	.083	.188	4.17
		30		.145	.085	.103	4.00
		50		.215	.041	.191	3.90
27.45	2.8	10	4.29	.115	.103	.089	4.21
		30		.271	.029	.203	4.04
		50		.365	.040	.255	3.84
27.33	5.6	10	4.27	.083	.125	.102	4.15
		30		.237	.044	.238	3.91
		50		.340	.015	.370	3.82
27.06	11.2	10	4.3	.062	.080	.170	4.15
		30		.225	.068	.254	3.92
		50		.321	.038	.347	3.77
41.60	2.8	10	4.39	.135	.101	.093	4.20
		30		.354	.042	.246	3.99
		50		.516	0	.255	3.77
41.45	5.6	10	4.3	.090	.126	.041	4.12
		30		.274	.046	.250	3.95
		50		.472	.014	.304	3.69
41.85	11.2	10	4.31	.076	.094	.240	4.18
		30		.266	.053	.308	3.92
		50		.443	.021	.477	3.77

TABLE 10 COMPARISON OF THE PREDICTED AND EXPERIMENTAL SHERWOOD NUMBERS

Temp. °C.	Equivalent Bubble Diameter	N_{Re}	N_{Sh}	
			Predicted	Experimental
15	0.228	816	307	304
	0.266	1029	344	346
	0.304	1193	370	402

TABLE 11 EFFECTS OF REACTION RATE CONSTANTS ON SHERWOOD NUMBERS PREDICTED BY THEORY (36)

N_{Sc}	N_{Re}	k_1	Average N_{Sh}	ϕ
89.5	1193	0	370	
		10	370	1.0
		40	370	1.0
		50	370	1.0
		100	370	1.0
		10^3	374	1.01
		10^4	471	1.27
		10^5	684	1.85
		10^6	1966	5.32

7. DISCUSSION OF RESULTS

7.1 Apparatus and Operation

The present apparatus (Figure 3) was designed to reduce to a minimum contamination of reactants and products by employing glass, type 316 stainless steel and Teflon as materials of construction. The exact nature of the plastic used in the solution metering pump was not known, but it was not visibly affected by continuous contact with the liquid reactants.

There were no major difficulties in operating this apparatus. However, a few improvements are possible. The Beckman solution metering pump, which gave a pulsating flow of the liquid, caused slight fluctuation of the column height. A constant-pressure feed tank might be used to eliminate this effect. The air flow rates could be regulated only to ± 1.5 c.c./min. of the desired value because of the insensitivity of the Swagelok needle valve. This could cause significant change in the slopes and intercepts of the N.T.U. vs. h plots.

Each straight line shown in Figures 5 to 7 constituted three data points, corresponding to data obtained from three different column heights. Additional data from one or two more column heights for each air flow rate would have reduced the error of the linear regression analysis. Unfortunately, the present apparatus was constructed to operate with three heights only.

Several experiments with identical operating conditions were repeated to check reproducibility. The results are shown in Table A-14 in Appendix A-6. The oxygen analyser readings for identical operating conditions differ by less than 10%. However, the discrepancies in mass transfer coefficients, K_L^*, range from 2.5% to 16.5%. Higher air flow rates tend to give higher discrepancies. This may be explained, in part, by the fact that at higher air flow rates, the slope of the N.T.U. vs. h plot is smaller than those at lower air flow rates. The same order of magnitude change in the slope causes a higher percent discrepancy in K_L^*.

Steady-state operation with respect to the gas phase was reached when the oxygen content in the exit gas as detected by the oxygen analyser remained unchanged with time. Three liquid samples were taken at approximately 30 minute intervals after steady state was reached in the gas phases and analysed for peracetic acid, AMP, acetic acid and acetaldehyde. These analyses showed, within experimental accuracy, that the concentrations of the above components remained constant with time. Hence, the constant reading of the oxygen analyser was considered a criterion for attainment of steady-state operation of the bubble reactor.

Cine pictures and single frame pictures were taken to determine the shape and behaviour of bubbles in the reactor column. These pictures were used to estimate the bubble velocity of rise and bubble frequency (See Appendix A-1). It was noted that the frequency of bubbles increased substantially from air flow rate of 10 c.c./min. to 30 c.c./min. Beyond this, the frequency increase was less noticeable. These observations conformed with the findings of other workers in this field (1, 14).

The volume of an individual bubble was estimated from the total air flow rate and the bubble frequency. In the calculation of the bubble diameter and surface area, the bubbles were assumed spherical. Photographic studies showed that the shape of the bubbles after corrections for optical distortion were ellipsoidal. However, the difference in surface area between a sphere and an ellipsoid of the same volume and having volumes equivalent to those of this investigation differ by less than 4%. Bubbles of the same volume rising in the same liquid will have the same shape.

7.2 Interpretation of Oxygen Transfer Data

The apparatus used in this study employed a single nozzle as an air inlet, and the bubbles generated were discrete and did not coalesce with one another. It might be expected that bubble formation at the nozzle and break-up at the top of the column had distinct effects on mass transfer. Such effects were evident as positive intercepts at zero column height were obtained from the N.T.U. vs. h plots. However, there were three cases where negative end effects were obtained as shown in Table 4. Such situations are considered physically impossible with the present apparatus. Their presence might be explained by the following argument. Each line shown in Figures 5 to 7 represented a least squares straight line fit on three data points. Figure A-5 shows the maximum deviation from an experimental data point governed by the accuracy of the oxygen analyser. A negative intercept would be obtained if a straight line was drawn through the maximum limit of one data point and the minimum limit of another.

The end effects for bubbles at low air flow rate (10 c.c./min.) were noticeably higher than those at higher air flow rates. At low air flow rates, the time required for a bubble to form at the nozzle was approximately twice as long as that at higher flow rates (30 - 50 c.c./min.) Hence formation effect on mass transfer apparently was larger.

An analysis of variance on the number of transfer units (see Table A-16) shows that N.T.U. is significantly affected by the changes in temperature, catalyst concentration, column height, air flow rate and the interactions of (temperature) x (column height), (catalyst concentration) x (column height), (catalyst concentration) x (air flow rate) and (column height) x (air flow rate). A regression analysis of N.T.U. with temperature, catalyst concentration, column height and air flow rate as independent variables shows that with 95 percent of confidence, a positive intercept exists at zero column height.

It is noted that the end effects enhanced mass transfer in the single-nozzle bubble reactor. The end effects will be further studied in the proposed multi-orifice bubble column. If appreciable end effects still exist, a future apparatus may be built to investigate bubble regeneration at intermediate levels in the column.

The mass-transfer coefficients with chemical reaction were estimated from the slopes of the straight lines shown in Figure 5 to 7. With the knowledge of bubble diameter and diffusivity of oxygen in the reaction mixture, the Sherwood numbers of the bubbles can be calculated. Table 10 compares the predicted Sherwood numbers with the experimental ones. Their agreement was satisfactory at low air flow rates when the bubbles were approximately spherical. However, at higher air flow rates,

the bubbles were noticeably deformed and were oscillating. The actual surface area of such bubbles was difficult to estimate, but they were definitely larger than the surface area of ellipsoids of the same volume.

The numerical solutions predict that the Sherwood numbers are insensitive to the changes in the reaction rate constants and the enhancement factors are essentially equal unity for dimensionless reaction rate constants up to 10^3 (see Table 11). Hence, the predicted Sherwood numbers and mass-transfer coefficients with chemical reaction are identical to the cases where only physical mass transfer takes place (see Table A-9), that is, K_L^* (predicted) increases with increased temperature and decreases with increased air flow rate. The analysis of variance on the experimental mass-transfer coefficients with chemical reaction (see Appendix A-8) indicates that K_L^* (experimental) changes significantly with changes in temperature, air flow rate, but the change in K_L^* is insignificant for changes in catalyst concentration. It is noted that only limited experiments were repeated to obtain an estimate of the reproducibility of experimental results. If more experiments were repeated, a better reproduction of results might be possible.

In analysing the results of this study, the concentration of dissolved oxygen in the bulk of the liquid was assumed negligible compared to the equilibrium concentration of oxygen at the interface. No direct measurements of oxygen concentration in the bulk of the liquid were made in this study, but it is shown in Appendix A-5 that the maximum limits of dissolved oxygen might be estimated using two methods:

(1) Zero end effect: When dissolved oxygen was present in the bulk of liquid, Y_ℓ might not be assumed negligible. A value of Y_ℓ might then be assigned to adjust the experimental data so that the straight line of the N.T.U. vs. h plot passed through the origin. It is physically impossible for the present apparatus to have negative end effects, hence the value of Y_ℓ required to adjust the experimental data in the described manner might be considered as maximum amount of dissolved oxygen in the bulk of the liquid.

(2) Kinetic consideration: Detailed kinetic data for oxidation of acetaldehyde are not available in literature. A first-order, reaction-rate constant for this reaction was proposed by Pang (35 This information has been used to estimate the maximum amount of oxygen in the bulk of the liquid.

Rate of oxygen absorption =

$$V_R \frac{dC}{dt} = k_1 C_{O_2} V_R \qquad (42)$$

where C_{O_2} is the concentration of oxygen in the bulk of the liquid.

Method (1) should be regarded with some reservation since negative end effects were observed in a few cases. Method (2) indicated that the maximum error in mass-transfer coefficients estimated from the results of this study was less than 25%.

An analysis of variance on the enhancement factor (see appendix A-8) shows that the changes in temperature, catalyst concentration and air flow rate do not cause significant change in ϕ. Table 6 shows that the enhancement factors for various temperatures, catalyst concentrations and air flow rates are essentially equal to unity. Pang (35) investigated

gas absorption with the same chemical system in a stirred cell with a plane gas-liquid interface and showed that the enhancement factor changed markedly with catalyst concentration. The velocity distribution in a stirred cell is not available and it is therefore not possible to predict a mass-transfer coefficient for such an apparatus. Velocity distributions for single bubbles in a bubble reactor are available and mass-transfer coefficients have been predicted (36). These predictions indicate that the enhancement factor depends strongly upon the distribution of velocity.

The enhancement factors found experimentally using the bubble reactor and the stirred cell differed markedly. This is to be expected considering the marked difference in mixing patterns in the two apparatuses.

7.3 Product Distribution

At the end of each experiment, a liquid sample was taken and analysed for peracetic acid, AMP, acetic acid and acetaldehyde. The analytical method used were identical to those described by Pang (35). The concentration of these components were very small and it was difficult to distinguish positively their differences between various sets of experimental conditions, hence no mathematical model was attempted to describe these results. Tables 7 to 9 summarize these results and the following trends were noted:

(A) At constant temperature, column height and catalyst concentration

  (i) the production of peracetic acid and acetic acid increased with air flow rate,

  (ii) the production of AMP decreased with air flow rate.

(B) At constant temperature and column height

(i) the production of peracetic acid decreased with catalyst concentration,

(ii) the production of acetic acid increased with catalyst concentration,

(iii) the change in production of AMP with catalyst concentration was inconclusive.

(C) At constant column height and catalyst concentration

(i) the production of peracetic acid increased slightly with temperature,

(ii) the changes in production of AMP and acetic acid with temperature were inconclusive.

The concentrations of the products were too small to allow a more detailed interpretation of experimental data for product distribution. The study of product distribution should be included as a goal of further investigation on the same chemical system.

8. CONCLUSIONS AND RECOMMENDATIONS

The mathematical model based on Houghton's work (36) can be used to describe satisfactorily the absorption rate in a bubble reactor containing a chain of discrete bubbles.

Statistical analysis indicates that the enhancement factor, Φ, obtained in this study does not change significantly with change in catalyst concentration. The magnitude of the enhancement factors for four-fold increase in catalyst concentration is essentially equal to unity. However, in the investigation of the oxidation of acetaldehyde in a stirred cell with plane interface, Pang (35) found that the enhancement factor increases from 4 to 16 for the same range of catalyst concentration. It may be concluded that the mass-transfer process in the oxidation of acetalydehyde is controlled by the hydrodynamic conditions.

The positive intercepts on the abscissa in the majority of the N.T.U. vs. h plots and the positive intercept from the regression analysis of N.T.U. with temperature, catalyst concentration, air flow rate and column height as independent variables indicate the presence of end effects in the bubble column employed in this study.

The present apparatus consists of a single nozzle and the bubbles generated are discrete and do not coalesce with one another. Furthermore air is saturated with ethyl acetate before reaching the reactor, it is assumed that there is no mass transfer from the liquid to the gas phase. However, in a commercial bubble reactor, it is likely to have multiple orifices for gas inlets, non-uniform bubble sizes, bubble coalescence,

recirculation of bubbles and evaporation of liquid inside the bubbles. The hold-up of bubbles may be so large that the assumption of zero concentration of solute in the bulk of the liquid may not be valid. The present mathematical model and experimental results have not incorporated such effects. It is recommended that a multi-orifice laboratory bubble reactor be built to investigate some of the above effects and to extend the mathematical model to include multi-component diffusion and bubble interferences.

The kinetics of the catalytic oxidation of acetaldehyde are uncertain. A separate program may be initiated to study the mechanism of such reaction.

The present apparatus may be used to carry out further studies on effects of acetaldehyde concentration and catalysts other than cobaltous acetate.

The concentrations of the products obtained in this study were too low to be analysed accurately. An apparatus which generates large surface area and can be operated at higher pressure may be used to obtain more accurate data on product distribution.

In order to obtain a better measure of the reproduction error in the analysis of variance, more experiments should be repeated at different conditions.

9. REFERENCES

1. Van Krevelen and Hoftijzer, P.J., Chem. Eng. Prog., 46, 29 (1950).
2. Haberman, W.L. and Morton, R.K., American Society of Civil Engineers Proceeding, No. 387, Jan. 1954.
3. Bowman, C.W., Ph.D. Thesis, University of Toronto, (1960).
4. Poutanen, A.A., Ph.D. Thesis, University of Toronto, (1959).
5. Coppock, P.D. and Meiklejohn, G.T., Trans. Instn. Chem. Engrs., 29, 75 (1951).
6. Leibson, I., Holcomb, E.G., Cacoso, A.G. and Jacmic, J.J., A.I.Ch.E.J., 2, 296 (1956).
7. Li, P.S., West, F.B., Vance, W.H., and Moulton, R.W., A.I.Ch.E.J., 11, 581 (1965).
8. Yoshida, F. and Akita, K., A.I.Ch.E.J., 11, 9 (1965).
* 9. Siemes, W., Gunther, K., Chem. Ing. Tech., 6, 389 (1956).
10. Datta, R.L., Napier, D.H., and Newitt, D.M., Trans. Instn. Chem. Engrs., (London) 28, 14 (1950).
* 11. Rosenberg, B., U.S. Navy Dept. Report 727 (1950).
* 12. Turner, G.M., Paper presented at the San Francisco Meeting, A.I.Ch.E. (Sept. 14, 1953).
13. Mahoney, J.F. and Wenzel, L.A., A.I.Ch.E.J., 9, 641 (1963.)
14. Jackson, R, The Chemical Engineers CE 107, May, 1964.
* 15 Hadamard, J., Compt. Rend., 152, 1735 (1911).
* 16. Rybczynski, B., Bull. Acad. Sci. Cracovie, 1 40 (1911).

17. Garner, F.H. and Hammerston, D., Chem. Eng. Sci., 3, 1 (1954).

18. Bond, N.W. and Newton, D.A., Phil. Mag., 5, 794 (1928).

19. Whitman, W.G., Chem. & Met. Eng., 29 146 (1923).

20. Hatta, S., Techol Repts. Tokoku Imp. Univ., 8, 1 (1928-1929).

21. Van Krevelen, D.W. and Hoftijzer, P.J., Chem. Eng. Prog., 44, 529 (1948).

22. Higbie, R., Trans. Am. Inst. Chem. Engrs., 31, 365 (1935).

23. Danckwerts, P.V., IEC., 43, 1461 (1951)

24. Toor, H.L. and Marchello, J.M., A.I.Ch.E.J., 4, 97 (1958).

25. Gilliland, E.R., Baddour, R.F. and Brian P.L.T., A.I.Ch.E.J., 4, 223 (1958).

26. Brian, P.L.T., Hurley, J.F. and Hasseline, E.H., A.I.Ch.E.J., 7, 226 (1961).

27. Brian, P.L.T., A.I.Ch.E.J., 10, 5 (1964).

28. Sherwood, T.K. & Pigford, R.L., Absorption and Extraction, McGraw Hill Book Co. Inc., N.Y., 1952, P. 317.

29. Phillips, B., Frostick Jr., F.C. and Starcher, P.S., J. Am. Chem. Soc., 79, 5982 (1957).

30. Bawn, C.E.H. and Williamson, J.B., Trans. Fara. Soc., 47, 721 (1951).

31. Bolland, J.L. and Gee, G., Trans. Fara. Soc., 42, 236 (1946).

32. Bolland, J.L. and ten Have, P., ibid., 43 201 (1947).

* 33. Twigg, C.H., Symposium - Oxidation Process in Chemical Manufacture, September (1961). Soc. Chem. Ind. (London).

34. Carpenter, B.H., IEC Process Design and Development, 4, 105 (1965).

35. Pang, K.H., Master's Thesis, McMaster University, (1965).

36. Johnson, A.I., Hamielec, A.E. and Houghton, W.T., Paper presented at the Symposium on Fundamentals of Interfacial Phenomena. 58th Annual Meeting of A.I.Ch.E. Philadelphia, Penn. Dec. 1965.

37. Hamielec, A.E. and Baird, M.H.I., Can. J. Chem. Eng., 40, 119 (1962).

* The original article was not reviewed by the author.

ACKNOWLEDGEMENT

The author is deeply grateful to Dr. A.I. Johnson and Dr. A.E. Hamielec for their guidance and encouragement throughout the course of this work. He also wished to thank Mr. W.T. Houghton for providing the numerical solutions of mass transfer from single gas bubbles.

The financial assistance provided by McMaster University is gratefully acknowledged.

APPENDIX

A-1 Photographic Studies of Bubble Frequency and Velocity of Rise

A-1.1 Description of Method

Cine pictures and single frame pictures, taken during the same experiments with a Bolex 16 mm cine camera and a Pentax 35 mm single frame camera, were used to measure bubble velocity of rise and bubble frequency. A General Radio Type 1531-A Strobotac was used to measure bubble frequency after the approximate range was established by photographic studies.

All pictures were taken with the shadow photographic technique by placing a No. 1 photoflood light approximately 12 inches behind the reactor column. The light was dispersed by an opague plastic screen. The cine pictures were taken at a speed of 64 fps (frames per sec.) with lens opening of f/11 and Ansco Versapan film was used. The single frame pictures were taken with f/5.6 lens opening and shutter speed of 1/500 sec., using Ilford FP3 film.

The speed of the Bolex camera was calibrated against a Thompson stop watch. Table A-1 shows the results of calibration

TABLE A-1 CALIBRATION OF SPEED OF BOLEX CINE CAMERA

Time (Sec.)	No. of Frames
1	-
2	66
3	67
4	66
5	66
6	65
7	64
8	63
9	61

The variation of speed at the beginning and end of the run was caused by acceleration and deceleration of the camera winding mechanism. Only pictures taken during the 2nd to the 6th second were used in analysing the photographic data. An average speed of the camera of 66 fps was used.

The frequency of the strobotac may be calibrated against power-line frequency. Such calibrations were carried out periodically during the time when experimental data were collected. It was found that little adjustments were required.

A-1.2 Estimation of Bubble Frequency

The results of the cine and single frame pictures were analysed as follows:

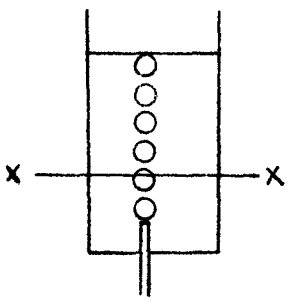

FIGURE A-1a

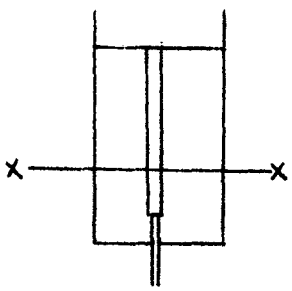

FIGURE A-1b

Figure A-1a represents the actual distribution of bubbles in the column. In Figure A-1b, these bubbles are imagined to be packed into a circular air cylinder that has the same height as the liquid column. A volume balance of the bubbles in Figure A-1a and Figure A-1b shows that

$$A'h = nV_B \qquad \text{(A-1)}$$

where

A' = cross-sectional area of imaginary air cylinder in Figure

A-1b. ($cm.^2$)

h = height of liquid column (cm.)

n = total number of bubbles in the liquid column

V_B = volume of a single bubble ($cm.^3$)

Therefore

$$A' = \frac{nV_B}{h} \tag{A-2}$$

Consider the volumetric flow rate of air which passes through plane x-x in Figures A-1a and A-1b,

$$fV_B = A' v_r \tag{A-3}$$

where

v_r = bubble velocity of rise (cm./sec.)

f = bubble frequency (1/sec.)

therefore

$$f = \frac{A'v_r}{V_B} \tag{A-4}$$

Substitute for A' using Equation (A-2)

$$f = v_r \frac{n}{h} \tag{A-5}$$

v_r is obtained from cine-picture studies, n is obtained from single frame pictures, and h is the liquid column height above the nozzle measured by a cathetometer. Table A-2 shows the results. The value of v_r for each air flow rate is an average of at least 8 observations from the cine pictures.

TABLE A-2 ESTIMATION OF BUBBLE FREQUENCY

(h = 12.5 in.)

Air flow rate $cm^3/min.$	n	n/h 1/cm.	v_r cm./sec.	$f = v_r \frac{n}{h} \times 60$ 1/min.
10	41	3.28	18.6	1600
30	81	6.49	20.1	3340
50	84	6.72	20.4	3480

A-1.3 Calculation of Equivalent Diameter and Equivalent Surface Area

The equivalent diameter, D_e, used in this study is defined as the diameter of the spherical bubble whose volume is equal to the volume of the actual bubble generated in the reactor. The equivalent surface area, S_e, is defined as the area of a sphere whose volume is equal to the volume of the actual bubble. The volume of an actual bubble

$$V_B = \frac{G}{n}$$

$$= \frac{4}{3}\pi r^3 \qquad \text{(A-6)}$$

$$= \frac{4}{3}\pi a^2 b$$

Therefore

$$D_e = 2r = 2\left(\frac{3V_B}{4\pi}\right)^{1/3} \qquad \text{(A-7)}$$

and

$$S_e = 4\pi r^2$$

$$= 4\pi\left(\frac{3V_B}{4\pi}\right)^{2/3} \qquad \text{(A-8)}$$

$$S = 2\pi a^2 + \frac{\pi b^2}{e} \ln \frac{1+e}{1-e} \qquad \text{(A-9)}$$

where e = eccentricity of ellipsoid = $\frac{\sqrt{\alpha^2 + \beta^2}}{\alpha}$. A comparison of S_e and S follows in Section A-1.4.

A-1.4 Correction for Bubble Distortion

The photographic studies showed that the shape of the bubbles were ellipsoidal. However, the minor and major axes of the bubble measured directly from the photographs were not true ones because of the distortion caused by the curvature of the reactor column and its cooling jacket. A spherical bead (0.6 cm. in diameter) was photographed under similar conditions in the column in place of a bubble. The measurements of the minor and major axes of the bead were used to correct for bubble distortion due to optical effects.

Table A-3 shows that the discrepancy between the actual surface area of an ellipsoidal bubble and the equivalent surface area is less than 4%.

TABLE A-3 BUBBLE DISTORTION

Bubble Volume ($cm.^3$)	Ratio of Major to Minor Axes: Actual Bubble	Ratio of Major to Minor Axes: Spherical Bead	Ratio of Major to Minor Axes: Corrected	Bubble Major Axis (cm.)	Bubble Minor Axis (cm.)	Equivalent Diameter D_e (cm.)	Equivalent Surface Area S_e (cm^2)	Actual Surface Area S (cm^2)
0.0063	1.65	1.4	1.18	0.121	0.1025	0.228	0.163	0.166
0.0100	1.65	1.4	1.18	0.142	0.120	0.266	0.221	0.227
0.0148	2.05	1.4	1.47	0.173	0.118	0.304	0.289	0.299

A-2 Experimental Details

A-2.1 Description of Apparatus

Figure A-2 is a schematic diagram of the continuous flow bubble column used in this study. The reactor column [1] was made of a 5/8 in. I.D. glass tube 26 in. long. Three sample outlets [2] were located at approximately 8 in., 13 in. and 18 in. from the bottom of the tube which was connected to a ℸ 24/40 ground glass joint.

The arrangements for reactant and air inlets are shown in Figure A-3. A machined Teflon plug [3] was fitted into the ground glass joint. At the bottom of the plug, two holes were drilled. The vertical hole [4] was tapped for 1/16" stainless steel Swagelok male connector. The nozzle for the air inlet was made of a 7 in. 0.028" O.D. stainless steel needle tubing [5] inserted into a 1/16" O.D. stainless steel tubing [6]. The tip of the nozzle was fitted with a 1/4" AWG #20 Teflon thin wall tubing [7]. The assembly was held in place by the 1/16" Swagelok male connector. The hole which was drilled 45° to the vertical, was tapped for 1/8" stainless steel Swagelok male connector and was used as the reactant inlet [8]. The reactor column [1] and the cooling jacket [10] were held together by means of rubber stoppers [11] and tie rods [12] as shown in Figure A-3.

The reactant column [1] was cooled by circulating chilled distilled water through the cooling jacket [10]. The distilled water was in turn cooled by ethylene glycol-water mixture from a Blue M Electric Co. Model PCC-4 1/3 HP refrigeration unit. The temperature of the distilled water was controlled by a Haake thermostat unit.

At the upstream of the reactor column [1], a 2 - litre flask [9]

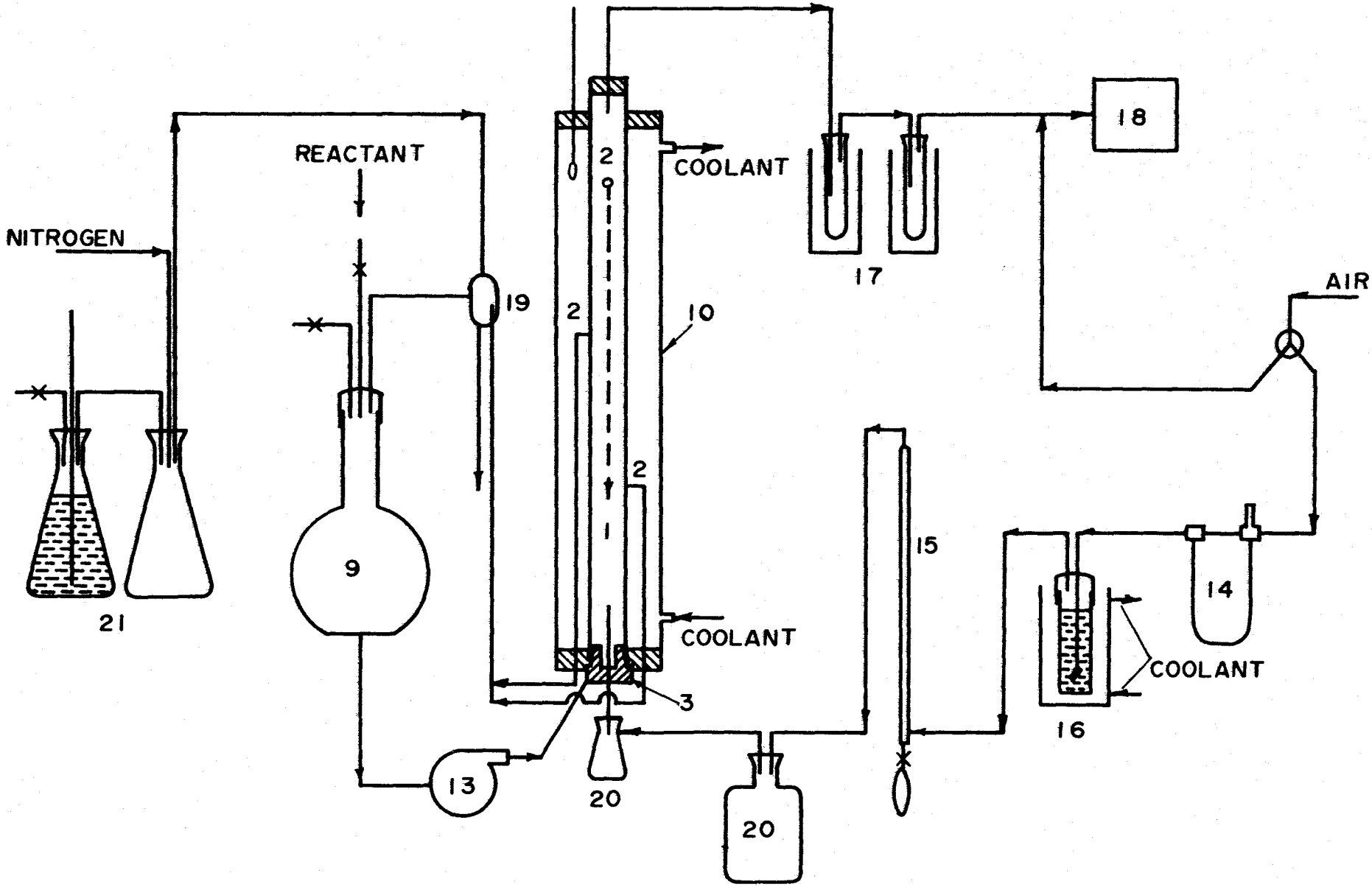

FIGURE A-2 SCHEMATIC DIAGRAM OF CONTINUOUS FLOW BUBBLE COLUMN

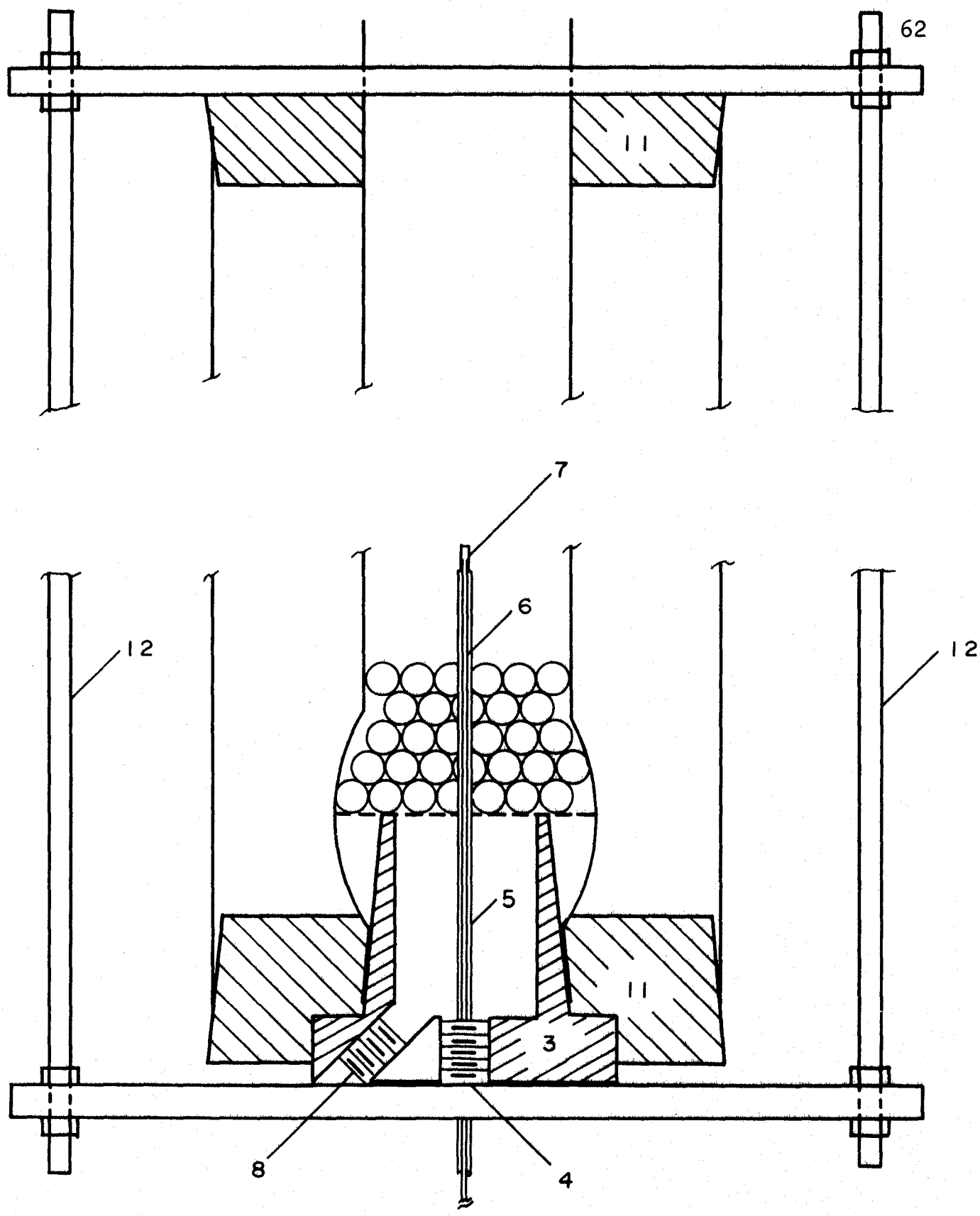

FIGURE A-3 DETAILS OF LIQUID REACTANT AND AIR INLETS

KEY TO FIGURES A-2 AND A-3

1	Reactor column
2	Reactant outlets
3	Teflon plug
4	Air inlet
5	Stainless steel needle tube
6	1/16" stainless steel tube
7	Teflon tip
8	Liquid reactant inlet
9	Reactant Reservoir
10	Cooling jacket
11	Rubber stoppers
12	Tie rods
13	Solution metering pump
14	Capillary flow meter
15	Soap-film meter
16	Air saturator
17	Dry ice-methanol cold traps
18	Oxygen analyser
19	Levelling device
20	Air chambers
21	Constant pressure bottles

with three inlets at the top was used as a reactant reservoir. One of the inlets was used to admit liquid reactants at the beginning of an experimental run. A second one, connected to a nitrogen cylinder, was used to purge the reservoir and also to keep the reactants blanketed with nitrogen throughout the experiment. The third inlet was used for the return of reactants in cases where the column was operated as a batch reactor.

The liquid reactants were led to the bottom of the column by means of a Beckman Model 726 solution metering pump [13], and ~~was~~ were then dispersed by a packing of glass beads before reaching the nozzle. Hence the bubbles formed at the nozzles were not disturbed by the incoming reactants.

The air used in this study was ordinary laboratory air filtered with a Cuno Micro-Klean filter. The air flow rate was regulated by a 1/8" Swagelok stainless steel needle valve and measured by a capillary flow meter [14]. The flow meter was periodically calibrated by an on-line soap film meter [15] made of a 50 c.c. burette. The incoming air was saturated with ethyl acetate before reaching the reactor, thus reducing the evaporation of reactants in the gas bubbles.

The exit gas passed through two dry ice-acetone cold traps [17] which condensed most of the organic vapours. The gas was then analysed by a Beckman Model 777 oxygen analyser [18]. The oxygen contents of the exit gas were recorded in a Bausch and Lomb laboratory recorder.

The out-flowing liquid products were led to a level controlling device [19] which might be raised or lowered to adjust the height of the liquid in the reactor column.

A-2.2 Experimental Procedure

A-2.2.1 Materials

The following chemicals were used in this oxidation study:

Cobaltous acetate (Fisher Scientific Co. Certified reagent grade).

Glacial acetic acid (Fisher Scientific Co. Certified reagent grade).

Ethyl acetate (Fisher Scientific Co. Certified reagent grade).

Acetaldehyde (Eastman Organic Chemicals, technical grade).

A-2.2.2 Preparation of Catalyst

Cobaltous acetate was used as catalyst in this study. In order to ensure a reproducible catalyst concentration, a fresh batch of standard catalyst was prepared before each experimental run.

The standard catalyst was prepared by dissolving 0.05 gm. of pulverized cobaltous acetate in 5.0 ml. of glacial acetic acid. The solution was made up to 50.0 ml. with ethyl acetate in a volumetric flask.

A-2.2.3 Preparation of the Reactant

The reactant solution contained 5% by volume of acetaldehyde in ethyl acetate. It was prepared by diluting 50.0 ml. of acetaldehyde with ethyl acetate and the solution was made up to 1000 ml. in a volumetric flask. Appropriate amounts of standard catalyst solution were added to the mixture, depending on the concentration of catalyst required for each experiment.

A-2.2.4 Experimental Procedure

At the beginning of every experiment, the reactant reservoir [12] was purged with nitrogen. The reactant was then poured into the reservoir and the solution metering pump [13] started. Air was admitted into the reactor column [1] before the reactants reached the nozzle to prevent the reactants from flowing back.

When the reactor column [1] was filled to the required height, the flow rate of the reactants was adjusted to 3.3 ml. per minute, and the air flow rate to the required value for the particular experiment. The oxygen content of the exit gas during the experiment was analysed and recorded. When steady state condition was achieved, a 15 ml. liquid sample was taken and analysed for peracetic acid, AMP, acetic acid and acetaldehyde. The analytical methods used were identical to those described by Pang (A-1). The system was considered to be at steady state when the chemical analyses of the liquid samples and the oxygen content of the exit gas did not change with time. It was found by repeated chemical analyses performed throughout the experiment that the liquid phase reached steady state when the oxygen content of the exit gas remained constant.

The bubble frequency was measured by a General Radio Type 1531-A strobotac.

A-3 Physical Properties

The viscosity, density and diffusivity of acetaldehyde and ethyl acetate mixtures are referred to throughout this thesis. The values of some of these properties for pure acetaldehyde and ethyl acetate and empirical formulae used to estimate properties of mixtures may be found in the following references: (A-2, A-3, A-4, A-5, A-6, A-7, and A-10).

The following abbreviations are used in this thesis:

AcH	≡ acetaldehyde	O_2	≡ oxygen
EtAc	≡ ethyl acetate	Mix	≡ acetaldehyde and ethyl acetate mixture

A-3.1 Density

The temperature range involved in this study (5° to 15°C.) is considered small and variations of density of the reactants with temperature have been neglected.

ρ_{AcH} at 18°C. = 0.783 gm./c.c. (Ref. A-3)

ρ_{EtAc} at 20°C. = 0.901 gm./c.c (Ref. A-3)

It was found that there was no appreciable change in volume when acetaldehyde and ethyl acetate were mixed. Density of the mixture according to volume fraction is

$$\rho_{Mix} = (\lambda\rho)_{AcH} + (\lambda\rho)_{EtAc}$$

$$= (0.05)(0.783) + (0.95)(0.901)$$

$$= 0.895 \text{ gm./c.c.}$$

$$x_{AcH} = \frac{(5)(0.783)/44}{(5)(0.783)/44 + (95)(0.901)/88}$$

$$= 0.0838$$

$$x_{EtAc} = 1 - x_{AcH}$$

$$= 0.9162$$

Therefore, density of the mixture according to mole fraction

$$\rho_{Mix} = (x\rho)_{AcH} + (x\rho)_{EtAc}$$

$$= (0.0838)(0.783) + (0.9162)(0.901)$$

$$= 0.892 \text{ gm./c.c.}$$

There is no significant difference in density of the mixture calculated according to volume fraction or mole fraction. A density of the mixture of 0.895 gm./c.c. has been used in this investigation.

A-3.2 Viscosity

The relationships between temperature and viscosity of acetaldehyde and of ethyl acetate are listed in the International Critical Tables (A-2). Reid and Sherwood (A-4) suggested the following formula to estimate the viscosity of the mixture:

$$\mu_{Mix} = x_1\lambda_1\mu_1 + x_2\lambda_2\mu_2 + 2(x_1x_2\lambda_1\lambda_2)\mu_{12} \qquad \text{(A-10)}$$

where μ_{12} is the viscosity of the interacting substance. In this case, μ_{12} is not available in the literature. The viscosity of the mixture was assumed to vary with the volume fraction of the individual components.

$$\mu_{Mix} = (\lambda\mu)_{AcH} + (\lambda\mu)_{EtAc} \qquad \text{(A-11)}$$

Therefore at 15°C.

$$\mu_{Mix} = 0.05(0.2325) + 0.95(0.476)$$

$$= 0.465 \text{ c.p.}$$

A No. 25 standardized Cannon-Fenske viscometer was used to check the viscosity of the acetaldehyde and ethyl acetate mixture (5% by volume of acetaldehyde). The viscosity of the mixture at 15°C.was found

to be 0.462 c.p. This value is within 1% of the predicted one.

TABLE A-4 VISCOSITY OF AcH-EtAc MIXTURE AT VARIOUS TEMPERATURES. (95% vol. EtAc)

Temperature °C.	μ_{AcH} c.p.	μ_{EtAc} c.p	μ_{Mix} c.p
5	0.2545	0.54	0.526
10	0.2435	0.506	0.493
15	0.2325	0.476	0.465

A-3.3 Diffusivity

The semi-empirical relation proposed by Wilke and Chang (A-5) was used to estimate the diffusivity of oxygen in acetaldehyde and ethyl acetate.

$$D_{AB} = 7.4 \times 10^{-8} \frac{(\lambda_B M_B)^{0.5} T}{\mu_B \bar{V}_A^{0.6}}$$

where

$\bar{V}_A$ = molar volume of solute A as liquid at its normal boiling point. c.c./g.mole.

The density of oxygen at -183°C is 1.14 gm./c.c. (A-10). Therefore $\bar{V}_{O_2} = M_{O_2} / \rho_{183} = 32/1.14 = 28.1$ c.c./g. mole. Both acetaldehyde and ethyl acetate may be considered as unassociated solvents, and the values of their "associative parameter", λ, is equal to 1.0. For T = 278°K

$$\mu_{AcH} = 0.2545 \text{ c.p.}$$

$$D_{O_2\text{-AcH}} = 7.4 \times 10^{-8} \frac{(1.0 \times 44)^{0.5}(278)}{(0.2545)(28.1)^{0.6}}$$

$$= 7.24 \times 10^{-5} \text{ cm.}^2/\text{sec.}$$

The diffusivity of A, the solute, in a multicomponent mixture is given by (A-6)

$$D_{A\text{-}Mix} = \frac{1}{(x_{B}/D_{AB}) + (x_{C}/D_{AC}) + (x_{D}/D_{AD}) + \cdots} \qquad \text{(A-13)}$$

Therefore, the diffusivity of oxygen in a mixture of acetaldehyde and ethyl acetate

$$D_{O_2\text{-}Mix} = \frac{1}{(0.0838/7.24 \times 10^{-5}) + (0.9162/4.82 \times 10^{-5})}$$

$$= 4.95 \times 10^{-5} \text{ cm.}^2/\text{sec.}$$

TABLE A-5 DIFFUSIVITY OF OXYGEN IN AcH-EtAc MIXTURE

Temperature °C.	D_{O_2} -AcH x10^5 cm^2/sec.	D_{O_2} -EtAc x10^5 cm^2/sec.	D_{O_2} - Mix x10^5 cm^2/sec.
5	7.24	4.82	4.95
10	7.68	5.23	5.37
15	8.21	5.66	5.8

A-4 Sample Calculations

A-4.1 Dimensionless Numbers

Reynolds number (N_{Re}) and Peclet number (N_{Pe}) of the bubbles and Schmidt number (N_{Sc}) are often referred to in analysing the experimental data. Their definitions and sample calculations are shown below:

$$N_{Re} = \frac{D_e \, v_r \rho_{Mix}}{\mu_{Mix}} \tag{A-14}$$

$$N_{Sc} = \frac{\mu_{Mix}}{\rho_{Mix} \, D_{O_2 - Mix}} \tag{A-15}$$

$$N_{Pe} = \frac{D_e \, v_r}{D_{O_2 - Mix}}$$

$$= N_{Re} N_{Sc} \tag{A-16}$$

For air flow rate of 10 c.c./min and at 5°C.

$$N_{Re} = \frac{(0.228)(18.60)(0.895)}{0.526 \times 10^{-2}} = 721$$

$$N_{Sc} = \frac{0.526 \times 10^{-2}}{(0.895)(4.95 \times 10^{-5})} = 119$$

$$N_{Pe} = (721)(119) = 85600$$

TABLE A-6 DIMENSIONLESS NUMBERS

Temperature °C.	Air Flow Rate c.c./min.	N_{Re}	N_{Sc}	N_{Pe}
5	10	721	119	85600
	30	910		108100
	50	1054		125600
10	10	753	103	77500
	30	970		99800
	50	1128		116000
15	10	816	90	73500
	30	1029		92700
	50	1193		107400

A-4.2 Solubility of Oxygen in Ethyl Acetate

Hildebrand and Scott (A-7) derived an empirical formula to evaluate the solubility of gases in non-electrolytes.

$$- \log c_2 = \log p_2^\bullet - \log p_2 + V_2(\delta_1 - \delta_2)/2.303\,RT \qquad \text{(A-17)}$$

where

c_2 = solubility of gas, mole fraction

$p_2^\bullet$ = vapour pressure of solute, atm.

p_2 = partial pressure of solute, atm.

V_2 = molal volume of solute at normal boiling point, c.c./g.mole

δ_1 = solubility parameter of solvent

δ_2 = solubility parameter of solute

The solubility parameter is defined as

$$\delta = \left(\frac{\Delta H^V - RT}{V}\right)^{0.5} \qquad \text{(A-18)}$$

where

ΔH^V = heat of vaporization, cal./g. mole

R = gas constant 1.98, cal./(g.mole)(°K.)

T = absolute temperature, °K

V = molal volume at normal boiling point, c.c./g.mole.

$\Delta H^V|_{EtAc}$ = 8970 cal./g.mole (Ref. A-2)

$\Delta H^V|_{O_2}$ = 1629 cal./g.mole (Ref. A-2)

$V|_{EtAc}$ = 97.7 c.c./g.mole

$V|_{O_2}$ = 28.1 c.c./g.mole

$$\delta|_{EtAc,5°C} = \left[\frac{8970 - (1.98)(278)}{97.7}\right]^{0.5}$$

$$= 9.29$$

$$\delta|_{O_2,5°C} = \left[\frac{1629 - (1.98)(278)}{28.1}\right]^{0.5}$$

$$= 6.19$$

The vapour pressure of solute may be calculated from the Clausius-Clapeyron equation. Hildebrand and Scott (A-7) gave the following equation:

$$\log p^\circ = \frac{\Delta H}{2.303R}\left(\frac{1}{T_b} - \frac{1}{T}\right) \qquad \text{(A-19)}$$

where T_b = normal boiling point °K.

Therefore, the vapour pressure of oxygen at 5°C

$$\log p^\circ = \frac{1629}{(2.303)(1.98)}\left[\frac{1}{90} - \frac{1}{278}\right]$$

$$= 2.68$$

According to equation (A-17), the solubility of oxygen in ethyl acetate at 5°C. may be calculated.

$$-\log x_2 = 2.68 - \log 0.21 + \frac{(28.1)(9.29 - 6.19)^2}{(2.303)(1.98)(278)}$$

$$= 3.571$$

$$x_2 = 2.69 \times 10^{-4} \text{ mole fraction}$$

TABLE A-7 SOLUBILITY OF OXYGEN IN ETHYL ACETATE

Temp °C.	δ_{EtAc}	δ_{O_2}	$\log p^\circ_{O_2}$	$x_2 \times 10^4$ mole fraction
5	9.29	6.19	2.68	2.69
10	9.29	6.17	2.71	2.51
15	9.28	6.15	2.73	2.41

The present apparatus was also used to check the solubility of

oxygen in ethyl acetate at 15°C. Air was bubbled through a 20.5 cm. column of ethyl acetate which was circulating at a rate of 3.3 c.c./min. At steady state, the rate of oxygen absorption was found to be independent of air flow rate. This indicated that the ethyl acetate was saturated with oxygen. The amount of oxygen absorbed may be considered as the solubility of oxygen in ethyl acetate.

The following summarizes the results of the solubility experiment:

Air flow rate c.c./min.	9.7	30.3
% O_2 in inlet gas	21.0	21.0
% O_2 in exit gas	19.4	20.5
O_2 flow rate at gas inlet c.c./min.	2.04	6.37
O_2 flow rate at gas outlet c.c./min.	1.85	6.18
O_2 absorbed c.c./min.	0.19	0.19
gm/min.	0.000258	0.000258
Ethyl acetate flow rate c.c./min	3.3	

Solubility of oxygen in ethyl acetate

$$= \frac{0.000258}{3.3} \quad \frac{\text{gm.}O_2}{\text{c.c. EtAc.}}$$

$$= \frac{0.000258/32}{0.901/88}$$

$$= 2.38 \times 10^{-4} \text{ mole } O_2\text{/mole EtAc.}$$

Therefore, the solubility of oxygen in ethyl acetate determined experimentally compares favourably with the predicted value shown in Table A-7.

A-4.3 Henry's Law Constant

Henry's law constant may be calculated from the solubility data of oxygen in ethyl acetate. Henry's law states that

$$Y = Hc \qquad \text{(A-20)}$$

where

Y = mole ratio of O_2 to N_2 moles of O_2/moles of N_2

c = solubility of O_2 moles of O_2/c.c. EtAc

H = Henry's Law constant

At 5°C.

$$c = \frac{2.69 \times 10^{-4}}{97.7}$$

$$= 2.75 \times 10^{-6} \text{ moles of } O_2/\text{ c.c. EtAc.}$$

Therefore $$H = \frac{0.21/0.79}{2.75 \times 10^{-6}}$$

$$= 0.967 \times 10^{5} \ \frac{\text{moles } O_2/\text{mole } N_2}{\text{moles } O_2/\text{c.c. EtAc}}$$

TABLE A-8 CALCULATED HENRY'S LAW CONSTANTS

Temp. °C.	Solubility of O_2 Mole O_2/c.c. EtAc	H $\frac{\text{mole } O_2/\text{mole } N_2}{\text{mole } O_2/\text{c.c. EtAc}}$
5	2.75×10^{-6}	0.967×10^{5}
10	2.58×10^{-6}	1.032×10^{5}
15	2.47×10^{-6}	1.078×10^{5}

A-4.4 Physical Mass Transfer Coefficients

Hamielec and Baird (A-8) showed that for circulating gas bubbles with thin boundary layer, the physical mass transfer coefficients may be estimated by Boussinesq equation

$$N_{Sh} = 1.13\ (N_{Pe})^{0.5} \qquad \text{(A-21)}$$

where

N_{Sh} = Sherwood number

$$= \frac{D_e k_L}{D_{O_2\text{-Mix}}}$$

The bubbles in this study were circulating because of the high Reynolds number and the assumption of thin boundary layer was valid for N_{Pe}>100. (A-8)

TABLE A- 9 CALCULATED PHYSICAL MASS TRANSFER COEFFICIENTS

Temp °C.	Air Flow Rate c.c./min.	N_{Sh}	D_e cm.	$D_{O_2\text{-Mix}} \times 10^5$ $cm^2/sec.$	$k_L \times 10^2$ cm/sec.
5	10	331	0.228	4.95	7.2
	30	372	0.266		6.92
	50	401	0.304		6.51
10	10	314	0.228	5.37	7.37
	30	356	0.266		7.18
	50	386	0.304		6.97
15	10	306	0.228	5.8	7.75
	30	344	0.266		7.52
	50	370	0.304		7.04

A-4.5 Mass Transfer Coefficient With Chemical Reaction

Material balance of oxygen transfer from the bubbles shows

$$-G_N dY = K_G^* a\ (Y - Y_\ell)\ dh \qquad \text{(A-22)}$$

where

G_N = flow rate of nitrogen, moles/sec.

Y = mole ratio of oxygen to nitrogen in bulk gas

Y_ℓ = mole ratio of oxygen to nitrogen of bulk gas in equilibrium with bulk liquid

K_G^* = gas phase mass transfer coefficient with chemical reaction

moles O_2/cm^2 sec.

a = bubble surface area per unit column height, cm^2/cm.

h = column height

It is assumed that the concentration of oxygen in the bulk of the liquid is negligible i.e. $Y >> Y_\ell$

Equation (A-22) is integrated to give

$$\ell n \frac{Y_{IN}}{Y_{OUT}} = \frac{K_G^* a}{G_N} h \qquad \text{(A-23)}$$

A plot of $\ell n\ (Y_{IN}/Y_{OUT})$ vs. h gives a straight line whose slope is equal to $K_G^*\ a/G_N$. The bubble surface area per unit column height, a, was estimated from photographic studies, and G_N was measured during the experiment, K_G^* might be calculated.

Example: Data taken from experiments 1501 to 1503.

Temperature = 15°C.

Catalyst Concentration = 5.6 ppm

Air flow rate = 10 c.c./min.

Henry's law constant = 1.078×10^5

Slope = 0.0302

G_N = 10 x 0.79/60

= 0.1318 c.c./sec.

$$= \frac{0.1318}{22400\ (288/273)}$$

$= 5.57 \times 10^{-6}$ mole/sec.

Therefore

K_G^* = (slope)(G_N/a)

$$= 0.0302\ (5.57 \times 10^{-6}/0.212)$$

$$= 0.793 \times 10^{-6} \text{ moles } O_2/(\text{sec})(\text{cm.}^2)$$

For resistances in series, the mass transfer coefficient may be related as

$$\frac{1}{K_G^*} = \frac{1}{k_G^*} + \frac{H}{k_L^*} \qquad \text{(A-24)}$$

and

$$\frac{1}{K_L^*} = \frac{1}{k_L^*} + \frac{1}{Hk_G^*} \qquad \text{(A-25)}$$

If the gas phase resistance, $1/k_G^*$, were assumed negligible, equations (A-24) and (A-25) become

$$\frac{1}{K_G^*} = \frac{H}{k_L^*} \qquad \text{(A-26)}$$

and

$$K_L^* = k_L^* \qquad \text{(A-27)}$$

Therefore,

$$K_L^* = HK_G^*$$

$$= (1.078 \times 10^5)(0.793 \times 10^{-6})$$

$$= 0.086 \text{ cm./sec.}$$

TABLE A-10 MASS TRANSFER COEFFICIENTS WITH CHEMICAL REACTION AT 5°C

Temp °C	cat. con. ppm	Air Flow Rate c.c/min.	N_2 Flow Rate c.c/sec.	N_2 Flow Rate mole/sec.x10^6	Slope	a	K_G^* x 10^6	H x10^{-5}	K_L^* cm/sec.
5	2.8	9.9	0.1303	5.72	0.0271	0.212	0.731	0.967	.0724
		29.4	0.387	16.97	0.0173	0.574	0.512		.0507
		48.3	0.637	27.95	0.0104	0.775	0.375		.0371
	5.6	10.2	0.1342	5.89	0.0296	0.216	0.807	0.967	.0800
		30.0	0.395	17.34	0.0264	0.584	0.785		.0777
		49.1	0.649	28.45	0.0193	0.785	0.700		.0693
	11.2	10.1	0.1332	5.84	0.0266	0.216	0.719	0.967	.0717
		29.2	0.385	16.90	0.0240	0.574	0.707		.0700
		48.5	0.638	28.0	0.0172	0.775	0.622		.0616

cat. con. = catalyst concentration

TABLE A-11 MASS TRANSFER COEFFICIENTS WITH CHEMICAL REACTION AT 10°C.

Temp	cat. con.	Air Flow Rate	N_2 Flow Rate		Slope	a	K_G^*	H	K_L^*
°C	ppm	c.c./min.	c.c./sec.	mole/sec.x10^6			x10^6	x10^{-5}	cm/sec.
10	2.8	10.1	0.133	5.74	0.0253	0.216	0.673	1.032	.0700
		29.9	0.394	17.0	0.0212	0.573	0.629		.0654
		48.5	0.635	27.4	0.0127	0.780	0.446		.0464
	5.6	10.1	0.133	5.74	0.0278	0.216	0.74	1.032	.0769
		30.0	0.395	17.04	0.0253	0.573	0.752		.0781
		49.0	0.645	27.8	0.0173	0.780	0.618		.0642
	11.2	10.1	0.136	5.86	0.0260	0.216	0.703	1.032	.0723
		28.5	0.371	16.0	0.0238	0.584	0.653		.0674
		49.2	0.638	27.5	0.0185	0.780	0.653		.0674

TABLE A-12 MASS TRANSFER COEFFICIENTS WITH CHEMICAL REACTION AT 15°C.

Temp	cat. con.	Air Flow Rate	N_2 Flow Rate		Slope	a	K_G^*	H	K_L^*
°C	ppm	c.c./min.	$\frac{c.c}{sec.}$	mole/sec x 10^6			x 10^6	x10^{-5}	cm/sec
15	2.8	9.4	0.124	5.25	0.0283	0.204	0.729	1.078	.079
		29.4	0.377	15.94	0.0244	0.564	0.690		.0748
		48.8	0.643	27.2	0.0208	0.775	0.730		.0792
	5.6	10.0	0.1318	5.57	0.0302	0.212	0.793	1.078	.086
		28.2	0.371	15.7	0.0246	0.555	0.695		.0754
		49.4	0.650	27.5	0.0197	0.795	0.682		.074
	11.2	10.0	0.1318	5.57	0.0299	0.216	0.771	1.078	.0836
		30.1	0.396	16.75	0.0242	0.580	0.700		.076
		48.5	0.639	27.05	0.0212	0.775	0.740		.0803

A-5 Effect of Dissolved Oxygen in Bulk of Liquid

If appreciable oxygen were present in the bulk of the liquid, Y_ℓ in equation (A-22) would not be negligible. Thus the driving force causing mass transfer from the gas bubbles to liquid would be reduced. The present study does not take into account oxygen concentration in the bulk of the liquid. Consequently, the estimation of mass transfer coefficients with chemical reaction, K_L^*, may be in error. Two methods are employed to establish an upper limit of this error.

A-5.1 Method 1 - Zero End Effect

The plots of N.T.U. vs. h as shown in Figures 5, 6, and 7 have positive intercepts on the abscissa. This may be considered an indication of end effects. If Y_ℓ were assumed to have a positive value instead of zero, a suitable value of Y_ℓ may be chosen to cause the $\ell n(Y_{IN}/Y_{OUT})$ vs. h plot to pass through the origin. The slope of this line may be used to calculate K_G^* as indicated in equation (A-23).

For air flow rate = 10.0 c.c./min.

catalyst concentration = 5.6 ppm

temperature = 15°C.

Y_ℓ = 0.035

Figure A-4 shows that the plot of $\ell n[(Y_{IN} - Y_\ell)/(Y_{OUT} - Y_\ell)]$ vs. h is a straight line whose slope is 0.0478 as compared to 0.0302 if Y_ℓ were assumed zero. The value of K_G^* is directly proportional to this slope. Therefore, if dissolved oxygen were present in the bulk of the liquid, the value of K_G^* might be changed by $\frac{0.0478 - 0.0302}{0.0302} \times 100\% = 58\%$.

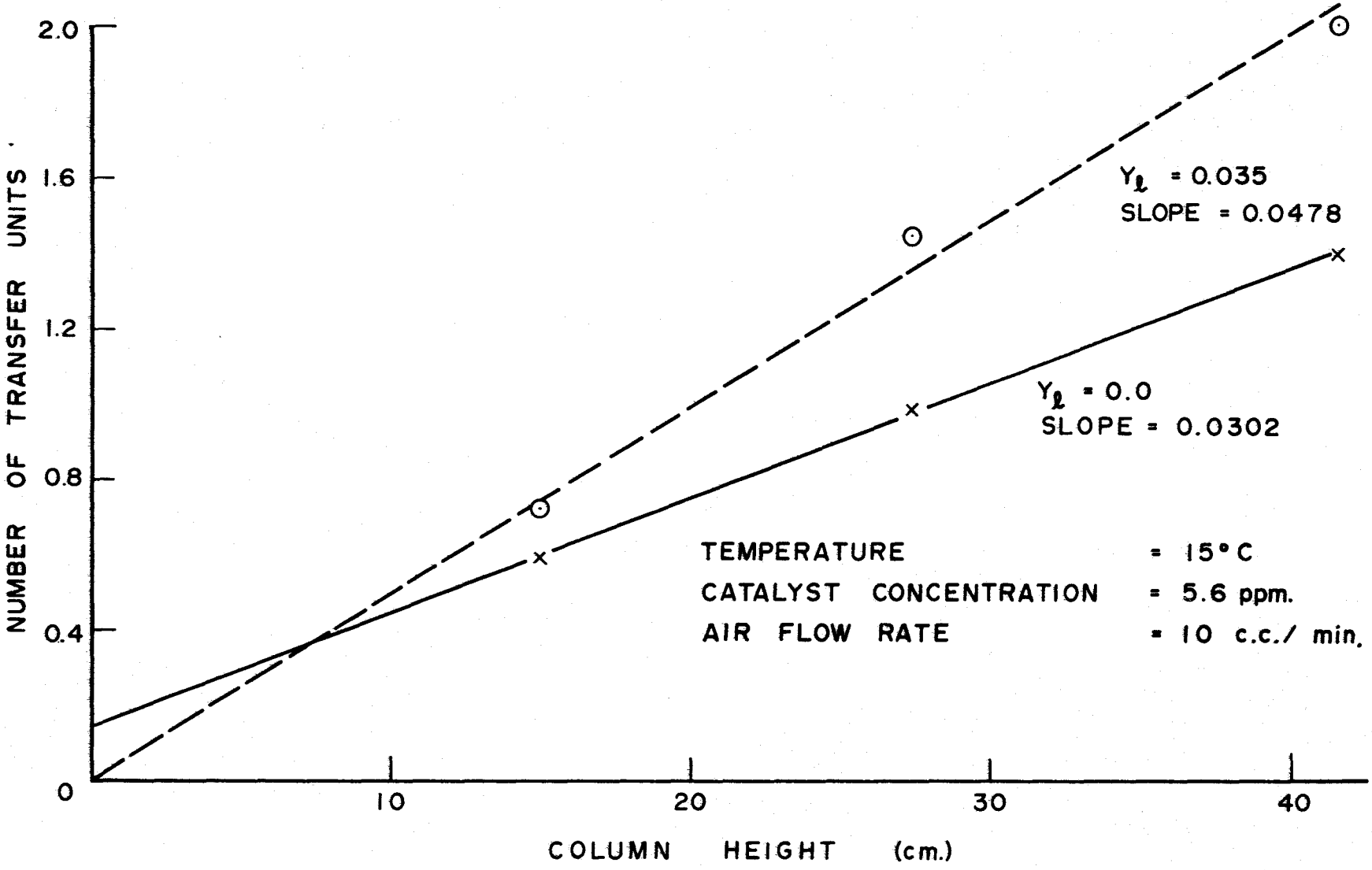

FIGURE A-4 EFFECT OF DISSOLVED OXYGEN IN THE BULK OF THE LIQUID

A-5.2 Method 2 - Kinetic Consideration

If the reaction rate constant of the oxidation of acetaldehyde were known, the maximum concentration of oxygen in the bulk of the liquid may be found from the following equation

$$V_R \frac{dC_{O_2}}{dt} = V_R k' C_{O_2}^{\ b}$$
$$= \text{rate of oxygen absorption} \qquad \text{(A-28)}$$

where V_R = volume of liquid in reactor, c.c.

C_{O_2} = concentration of oxygen in bulk of liquid, gm./c.c

k' = reaction rate constant

b = order of reaction

The rate of oxygen absorption and reactor volume, V_R, were measured experimentally. If the order of reaction and the reaction rate constant are known, equation (A-28) may be solved to give an upper limit to C_{O_2}.

Pang (A-1) obtained a pseudo-first order reaction rate constant, k_1, of this reaction using pure oxygen

$k_1 = 156\ hr^{-1}$

temperature = 15°C.

acetaldehyde concentration = 0.0675 mole fraction

catalyst concentration = 3 ppm.

Under similar conditions, the following data were obtained from the present apparatus using air:

Rate of oxygen absorbed = 0.00127 gm./~~c.c.~~ min.

Volume of liquid in reactor = 30.2 c.c.

According to equation (A-28)

$$C_{O_2} = \frac{0.00127}{156/60 \times 30.2}$$

$$= 0.000016 \text{ gm./c.c.}$$

$$= 0.445 \times 10^{-6} \text{ mole } O_2/\text{c.c}$$

which is an upper limit.

The mass transfer coefficient is defined as:

$$N_{O_2} = K_L^* \text{ (driving force)} \qquad \text{(A-29)}$$

If the concentration of oxygen inthe bulk of the liquid were assumed negligible, then the driving force for mass transfer will be equal to the concentration of oxygen at the gas liquid interface or the solubility of oxygen at the particular temperature. (2.47×10^{-6} mole O_2/c.c. at 15°C.)

If the concentration of oxygen in the bulk of the liquid were assumed as 0.445×10^{-6} mole O_2/c.c., the driving force for mass transfer would be $(2.47 - 0.445) \times 10^{-6}$ mole O_2/c.c.

Therefore, with the presence of dissolved oxygen in the bulk of the liquid, the value of K_L^* would be increased by

$$\frac{0.445}{(2.47 - 0.445)} \times 100\% = 22\%$$

This is the maximum value for k_L^* due to the assumption that the concentration of oxygen in the bulk of liquid is negligible

A-6 Experimental Error

The Beckman model 777 oxygen analyser has an accuracy of ± 1% of the full scale at constant temperature. The scale of 0 to 25 per cent of oxygen was used during the experimental runs. Therefore, the error caused by the oxygen analyser was ± 0.25% of oxygen in the sample. Table A-13 and Figure A-5 shows the maximum possible spread of experimental results.

The data were taken from experiments under the following conditions:

Temperature = 15°C.

Catalyst concentration = 5.6 ppm.

Air flow rate = 10 c.c./min.

A-6.1 Reproducibility

A set of experiments with the following conditions were repeated to check the reproducibility of results.

Temperature = 10°C.

Catalyst concentration = 11.2 ppm.

Acetaldehyde concentration = 5% (by volume)

Table A-14 shows the mass transfer coefficients, K_L^*, calculated from the two sets of experimental results. It indicates that the results may be reproduced within 20%.

TABLE A-13 MAXIMUM SPREAD OF EXPERIMENTAL RESULTS

Column Height cm.	15.0		
% Oxygen in Exit Stream (A)	12.55	12.8	13.05
% Nitrogen in Exit Stream (B)	87.45	87.2	86.95
Y_{OUT} (A)/(B)	0.144	0.147	0.150
Y_{IN}/Y_{OUT}	1.85	1.81	1.78
$\ell n(Y_{IN}/Y_{OUT})$	0.615	0.594	0.574
Column Height cm.	27.3		
% Oxygen in Exit Stream (A)	8.75	9.0	9.25
% Nitrogen in Exit Stream (B)	91.25	91.0	90.75
Y_{OUT} (A)/(B)	0.096	0.099	0.102
Y_{IN}/Y_{OUT}	2.77	2.69	2.61
$\ell n(Y_{IN}/Y_{OUT})$	1.02	0.99	0.96
Column Height cm.	41.5		
% Oxygen in Exit Stream (A)	5.95	6.2	6.45
% Nitrogen in Exit Stream (B)	94.05	93.8	93.55
Y_{OUT} (A)/(B)	0.063	0.066	0.069
Y_{IN}/Y_{OUT}	4.22	4.03	3.86
ℓn (Y_{IN}/Y_{OUT})	1.44	1.40	1.35

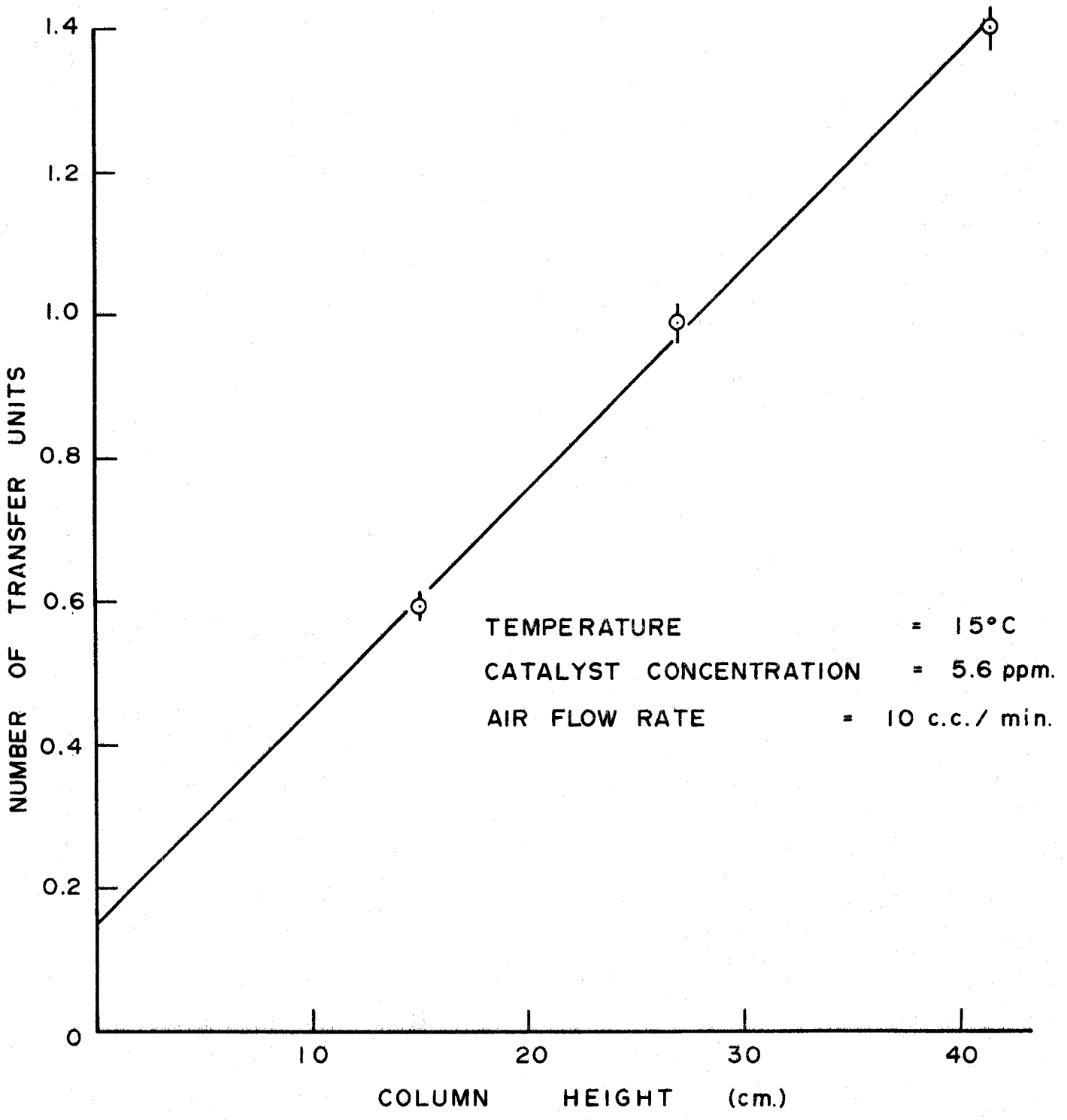

FIGURE A-5 MAXIMUM SPREAD OF EXPERIMENTAL RESULTS

TABLE A-14 REPRODUCIBILITY OF EXPERIMENTAL RESULTS

TEMPERATURES = 10°C

CATALYST CONCENTRATION = 11.2 ppm.

Air Flow Rate cc/min	Experimental Set A					Experimental B					Discrepancy in K_L^* %
	Column Height cm.	Oxygen Analyser Reading %	$\ln \frac{Y_{IN}}{Y_{OUT}}$	Slope	K_L^* cm/sec	Column Height cm.	Oxygen Analyser Reading %	$\ln \frac{Y_{IN}}{Y_{OUT}}$	Slope	K_L^* cm/sec	
10	18.65	11.2	.746	.0256	.0707	15.42	11.5	.719	.0260	.0725	2.5
	27.16	9.3	.955			27.62	9.1	.980			
	41.34	6.6	1.326			42.05	6.1	1.41			
30	18.65	12.7	.604	.0187	.0574	15.42	13.9	.495	.0238	.0674	14.8
	27.16	11.0	.765			27.62	10.7	.797			
	41.34	8.4	1.030			42.05	7.9	1.13			
50	18.65	14.0	.489	.0153	.0563	15.42	15.0	.405	.0185	.0674	16.5
	27.16	12.5	.621			27.62	12.1	.658			
	41.34	10.3	.837			42.05	9.8	.900			

A-7 Numerical Solution of Mass Transfer From Gas Bubble

Houghton's(A-9) numerical solutions predicting Sherwood Numbers of gas bubbles in liquid are applied to the present work. Houghton's work was concerned with bubbles of low and intermediate Reynolds numbers. For his solutions, the Stokesor Hadamard velocity profiles were used for low Reynolds Numbers whereas Hamielec's extension of Kawaguti's velocity profiles were used for intermediate Reynolds numbers.

The present study involved Reynolds numbers ranging from 800-1200, hence the velocity profiles describing potential flow were used in the numerical solutions.

The following equation was developed from mass balance of a spherical element

$$V_r \frac{\partial C}{\partial r} + \frac{V_\theta}{r} \frac{\partial C}{\partial \theta} = D\left[\frac{\partial^2 C}{\partial r^2} + \frac{2}{r}\frac{\partial C}{\partial r} + \frac{\cot\theta}{r^2}\frac{\partial C}{\partial \theta} + \frac{1}{r^2}\frac{\partial^2 C}{\partial \theta^2}\right] - k_1 C \qquad \text{(A-30)}$$

Equation (A-30) is transformed into dimensionless form using the following definitions

$$r' = \frac{r}{R_b}\ ;\quad C' = \frac{C}{C_s}\ ;\quad V_r' = \frac{V_r}{U}\ ;\quad V_\theta' = \frac{V_\theta}{U}\ ;\quad k_1' = \frac{R_b^2 k_1}{D}\ ;\quad Pe = \frac{2R_b U}{D}$$

and becomes (primes are dropped)

$$V_r \frac{\partial C}{\partial r} + \frac{V_\theta}{r}\frac{\partial C}{\partial \theta} = \frac{2}{Pe}\left[\frac{\partial^2 C}{\partial r^2} + \frac{2}{r}\frac{\partial C}{\partial r} + \frac{\cot\theta}{r^2}\frac{\partial C}{\partial \theta} + \frac{1}{r^2}\frac{\partial^2 C}{\partial \theta^2} - k_1 C\right] \qquad \text{(A-31)}$$

The boundary conditions are

$$C = 1 \quad \text{at } r = 1$$

$$C = 0 \quad \text{at } r = \infty \qquad \text{(A-32)}$$

$$\frac{\partial C}{\partial \theta} = 0 \quad \text{at } \theta = 0, \pi \quad \text{axisymmetric flow}$$

The stream function in spherical coordinate and dimensionless form is:

$$\psi = (A\, r^2 + \frac{B}{r})\, \sin^2 \theta \qquad \text{(A-33)}$$

and the velocity profiles for potential flow may be expressed as:

$$V_r = \frac{-1}{r^2 \sin\theta} \frac{\partial \psi}{\partial \theta} \qquad \text{(A-34)}$$

$$V_\theta = \frac{1}{r \sin\theta} \frac{\partial \psi}{\partial r} \qquad \text{(A-35)}$$

Differentiating equation (A-33) with respect to θ and r and substitute into equations (A-34) and (A-35) to obtain

$$V_r = -[2A + \frac{2B}{r^3}]\, \cos\theta \qquad \text{(A-36)}$$

$$V_\theta = [2A - \frac{B}{r^3}]\, \sin\theta \qquad \text{(A-37)}$$

At $r = 1$ $V_r = 0$

equation (A-36) may be solved to obtain

$$A = -B \qquad \text{(A-38)}$$

At $r = \tau$ $\psi = \frac{1}{2}\, r^2 \sin^2 \theta$ (A-39)

Combine equation (A-33), (A-38) and (A-39) to obtain

$$A = \frac{1/2\, r^2}{r^2 - 1/r} \qquad \text{(A-40)}$$

As $r \rightarrow \infty$ $A \doteq 1/2$ and $B \doteq -1/2$

Substitute values A and B into equations (A-36) and (A-37) to obtain

$$V_r = -[1 - \frac{1}{r^3}]\, \cos\theta \qquad \text{(A-41)}$$

$$V_\theta = [1 + \frac{1}{2r^3}] \sin\theta \qquad \text{(A-42)}$$

The assumptions made in the numerical solutions are listed by Houghton (36).

Table A-15 shows the effect of reaction rate constants on Sherwood number. It is noted that the enhancement factor, Φ, does not change appreciably below reaction rate constant of 1000.

TABLE A-15 THE EFFECT OF DIMENSIONLESS REACTION RATE CONSTANTS ON AVERAGE SHERWOOD NUMBERS

N_{Sc}	N_{Re}	k_1	Avg. N_{Sh}	Φ
89.5	1193.0	0.0	370.0474	
		40.0	370.1981	1.0
		50.0	370.2405	1.0
		100.0	370.4370	1.0
		1,000.0	373.8909	1.01
		10,000.0	407.6662	1.10
		100,000.0	684.4190	1.85
		1,000,000.0	1965.9878	5.31
		10,000,000.0	Too high	

A-8 Statistical Analysis

Analyses of variance were carried out on the number of transfer units (N.T.U.), the experimentally determined mass-transfer coefficients (K_L^*) and the enhancement factor (ϕ) taking temperature, catalyst concentration, air flow rate, column height and their combinations as sources of variables. For analyses on K_L^* and ϕ, the column height was not a source variable. The results from the duplicated set of experiments performed at 10°C. and catalyst concentration of 11.2 ppm. were used to obtain an estimate of reproducibility error. The interaction terms when found insignificant individually were pooled together as a residual error.

The results of the anlayses of variance on the number of transfer units, mass-transfer coefficient, and enhancement factor are shown in Tables A-16 to A-18.

A regression analysis of the number of transfer units with temperature, catalyst concentration, air flow rate and column height as independent variables shows with 95 percent confidence, a positive intercept exists at zero column height. It is assumed that the independent variables have first order effects on N.T.U. Second order effects of the catalyst concentration ~~was~~ were also tried, but the relationship between N.T.U. and the variables does not change appreciably.

The resulting expression is

$$\begin{aligned} N.T.U. = {} & 0.188 + 0.308 \times 10^{-2}\,(TEMP) - 0.237 \times 10^{-3}(CAT) \\ & + 0.258 \times 10^{-1}(COL) - 0.552 \times 10^{-2}(ARATE) \\ & + 0.309 \times 10^{-3}(TEMP) \times (COL) + 0.236 \times 10^{-3}(CAT) \times (COL) \\ & + 0.307 \times 10^{-3}(CAT) \times (ARATE) - 0.262 \times 10^{-3}\,(COL) \times (ARATE). \end{aligned}$$

TABLE A-16 ANALYSIS OF VARIANCE ON N.T.U.

SOURCE	d.f.	S.S.	M.S.	F Calculated	$F_{0.05}$ Tabulated
TEMP	2	0.180194	0.090097	86.966	3.19
CAT	2	0.244586	0.122293	118.043	3.19
COL	2	4.931636	2.465818	2380.133	3.19
ARATE	2	2.420317	1.210158	1168.106	3.19
(TEMP) X (CAT)	4	0.004274	0.001068	1.031	2.56
(TEMP) X (COL)	4	0.027880	0.006970	6.728	2.56
(TEMP) X (ARATE)	4	0.004817	0.001204	1.162	2.56
(CAT) X (COL)	4	0.021645	0.005411	5.223	2.56
(CAT) X (ARATE)	4	0.032110	0.008028	7.749	2.56
(COL) X (ARATE)	4	0.163624	0.040906	39.485	2.56
ERROR	48	0.049731	0.001036		
TOTAL	80	8.080814			

d.f. = degrees of freedom

S.S. = sums of squares

M.S. = mean sums of square

TEMP = temperature

CAT = catalyst concentration

COL = column height

ARATE = air flow rate

$F_{0.05}$ = 0.05 probability of a larger value of F.

Note: Table A-16 does not include results from duplicated experiments.

TABLE A-17 ANALYSIS OF VARIANCE ON EXPERIMENTAL K_L^*

SOURCE	d.f	S.S	M.S.	F calculated	$F_{0.05}$ tabulated
TEMP	2	10.3860	5.1930	13.7599	9.55
CAT	2	6.3171	3.1586	8.3694	9.55
ARATE	2	8.0917	4.0458	10.7202	9.55
REPRODUCTION ERROR	3	1.1323	0.3774		
RESIDUAL ERROR	20	10.0735	0.5367		
TOTAL	29	36.0006			

TABLE A-18 ANALYSIS OF VARIANCE ON ϕ

SOURCE	d.f	S.S	M.S.	F calculated	$F_{0.05}$ tabulated
TEMP	2	0.1026	0.0513	6.75	9.55
CAT	2	0.1267	0.0634	8.34	9.55
ARATE	2	0.0531	0.0266	3.50	9.55
REPRODUCTION ERROR	3	0.0228	0.0076		
RESIDUAL ERROR	20	0.2386	0.0119		
TOTAL	29	0.5438			

The standard error estimate is 0.041 with 72 degrees of freedom. Therefore, the confidence range of the intercept at zero column height at 5% probability is $0.188 \pm (2.0)(0.041)$ or from 0.106 to 0.270.

A-9 References

A-1 Pang, K.H., Master's Thesis, McMaster University, (1965).

A-2 International Critical Tables, Vol. 7, pp.213-215.

A-3 Perry, J. H., ed. Chemical Engineering Handbook, 4th ed. p. 3-23; p. 3-33.

A-4 Reid, R. C. and Sherwood, T. K. The Properties of Gases and Liquids, McGraw Hill Book Company, Inc., N. Y.,(1958) p. 217.

A-5 Wilke, C. R. & Chang, P., A.I.Ch.E.J., 1,264-270,(1955).

A-6 Treybal, R. E., Mass Transfer Operation, McGraw Hill Book Company, Inc., N. Y.,(1955) p. 19.

A-7 Hilderbrand, J. H. & Scott, R. L., The Solubility of Non-Electrolytes, Reinhold Publishing Corporation,(1950) p. 244, 424.

A-8 Hamielec, A. E. and Baird, M. H. I., Can. J. of Chem. Eng., 40, 119 (1962).

A-9 Johnson, A. I., Hamielec, A. E., Houghton, W. T. Paper presented at the Symposium on Fundamentals of Interfacial Phenomena. 58th Annual Meeting of A.I.Ch.E. Phildadelphia, Penn., December 1965.

A-10 Handbook of Chemistry and Physics, 43rd ed. The Chemical Rubber Publishing Co., Cleveland, (1962) p.2164.

A-11 Volk, W., Applied Statistics for Engineers, McGraw Hill Book Company, Inc., N.Y. (1958) pp. 136-223.